Discrete time measurement induced quantum random walks

Behaviour on elementary graphs

by

Julian Scheper

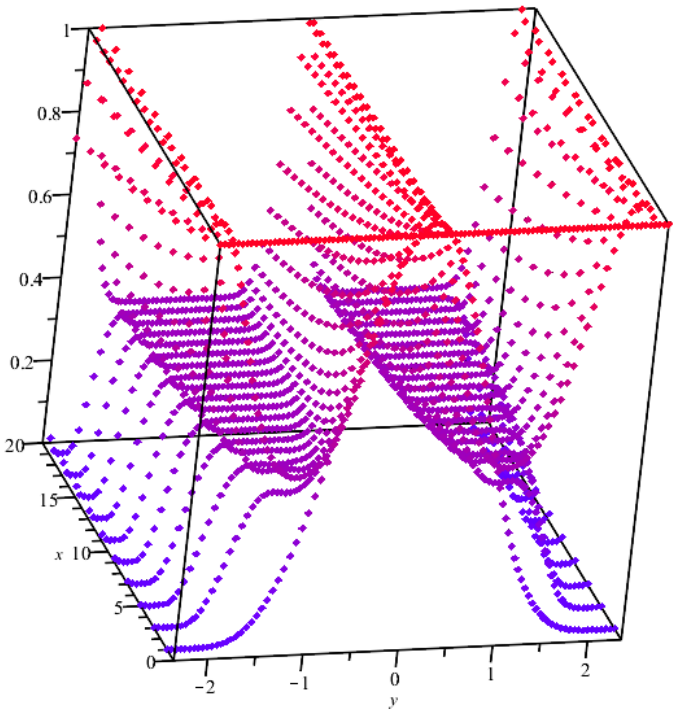

Supervisors: Johan Dubbeldam, Tim Taminiau
Institution: Delft University of Technology
Project Duration: February, 2022 - July, 2022

TU Delft

Abstract

Quantum random walks could play an important role in the algorithms used by quantum computers in the future, for example by replacing classical random walks in cases where this reduces computation time. In order to better understand 'Discrete Time Measurement Induced Quantum Random Walks' we investigate the walk on several elementary structures. On every structure, 'critical sampling rates' are discovered. These sampling rates are rates of measurement at which the behaviour of the quantum random walk on the structure differs drastically from the behaviour at other sampling rates. Hence the rate of measurement is crucial for the behaviour of quantum random walks. It is found that, on many structures, the critical sampling rates cause a 'break' of the structure into several sub-structures, a phenomenon which occurs only in quantum random walks. The breaks correspond to the divisors of the amount of nodes in the case of ring structures, implying that prime number rings do not have this breaking property in the same way that other rings do.

Larger systems such as a double ring and a double tree-graph are briefly discussed. In the case of the double tree-graph a critical sampling rate is found which breaks off the starting and end point of the tree, causing the walk to traverse the graph much faster than the classical random walk.

The term 'faster' is made concrete on the simpler systems by using analytical equations to calculate the expected amount of measurements $\langle n \rangle$ before measuring the walk at a desired node. In this thesis, only return problems are considered. Hence the desired node is always the starting node. Investigation of similarities and differences between the transition problem and the return problem could be the subject of further research.

Some general properties of the quantum random walk are investigated as well. Every structure is defined by its Hamiltonian. It will be shown, however, that the eigenvalues of this Hamiltonian are not enough information to find the exceptional sampling rates of the quantum random walk on the structure. But the eigenvalues can be used to check that the results are correct. In order to find the critical sampling rates the eigenvalues of a different matrix called G (the time-evolution matrix) need to be found. A possible way to find these eigenvalues consistently (for ring structures) is shown. Finally, the important result that G is a real symmetric matrix is proved, under the condition that the Hamiltonian H is also symmetric (as is usually the case).

Contents

1 Introduction

Recently ”Quantum Computers” are making the news, as more and more working prototypes are constructed around the world[7]. Quantum Computing promises to drastically improve the performance of current computers on several areas (in some cases exponentially reducing calculation time[5]), but to do this a quantum computer needs quantum software. Classical software is designed to be used efficiently by classical computers, and as a consequence, it does not make use of the new and different possibilities a quantum computer might have.

One example of a classical algorithm is the ”Random Walk”. This is a random process which is sometimes used by classical computers. A quantum computer can also make use of this Random Walk, but in some cases it is beneficial to use a ”Quantum Random Walk” instead. A quantum random walk is a different random process, which a quantum computer can use efficiently, but a classical computer cannot.

The idea of a ’quantum random walk’ might seem vague, but its existence has been demonstrated before in several different experiments. In, for example, [1] an ’optical Galton board’ is used. A Galton board is a device which can be used to model the classical random walk. The wave-like nature of light causes interference in the optical version of the Galton board. Due to this interference the probability distribution is changed from the distribution of a classical random walk to the distribution we expect from a quantum random walk. In [2], bosonic atoms in an optical lattice are used to demonstrate that again the behaviour of certain physical systems corresponds to the theory of quantum random walks. A short introduction to (quantum) random walks is given in chapter 2. More elaborate information can be found in for example [3].

This thesis aims to further explore the properties of one such quantum random walk, the ’Discrete Time Measurement Induced Quantum Random Walk’, which is introduced in [4]. In particular, we will look at the properties of the walk on elementary structures. The ’Discrete Time Measurement Induced Quantum Random Walk’, which will be referred to as simply ’Quantum random walk’ or ’Quantum walk’ in the rest of the thesis, is applied to ring structures consisting of 2, 3, 4, 5, and 6 nodes in chapter 4. Here, the quantum random walk is also applied to the ’Three node line’, and to two slightly larger systems: the double ring and the double tree-structure.

It will become clear that the rate of measurement is important for the behaviour of the quantum walk (hence the ’measurement induced’ part of the name). At some rates the behaviour changes drastically. These rates are called ’critical sampling rates’ and they will be discussed more extensively per structure in chapter 4. In order to make the discussion of critical sampling rates more exact some mathematics needs to be defined and derived, which is done in chapter 3. Finally, in chapter 5, some general properties of the quantum walk are discussed and proved.

2

Random walks

2.1. Classical random walks

Perhaps the most well-known classical random walk is the discrete time random walk on an infinite line. This random walk starts at a certain node ”0” on an infinite string of nodes. To the right the nodes are numbered ”1,2,3,...” and to the left ”-1,-2,-3,...”, as in figure 2.1.

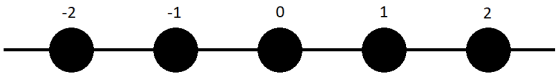

Figure 2.1: A schematic visualisation of the classical random walk on the infinite line.

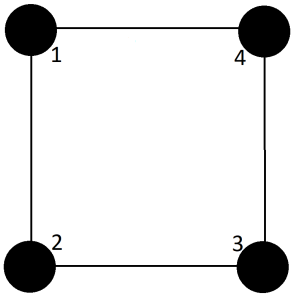

Figure 2.2: A schematic visualisation of the classical random walk on the square.

As mentioned, the classical random walk starts at node 0. Then, in the next time step, it either ”jumps” one position to the left, or one position to the right. Hence at time-step 1 it has a 50% chance of being at node 1, and a 50% chance of being at node -1. This process is repeated such that at time-step 2 the walk has a 25% of being at node 2, a 50% chance of being at node 0, and a 25% chance of being at node -2.

But random walks are possible on many structures, not just infinite lines. Another possible structure is the square, see figure 2.2. The important difference is that on this structure the walk can return to, for example, node 1 not only by first going to the right side and then back (as it could in the case of a line as well), but also by going right four times in a row. These two options (together with all other ways of getting back to node 1) then ’interfere’ at node 1. In the classical case this means that the probability of the walk being at node 1 at time t is equal to the sum of the probabilities of all the ways to get to node 1 at time t. Therefore the probabilities of all the possibilities interfere constructively.

The fact that the probabilities always interfere constructively seems intuitive, but it is not true in the case of the quantum random walk. The quantum random walk can interfere with itself constructively (same as the classical walk), but it can also interfere destructively. For example it is possible that, if the quantum random walk can get to a node via two different ways, the total probability of the walk being found at the node adds up to zero. An example of this happening can be found in section 4.1.3.

2.2. Quantum random walks

The discrete time quantum random walk is similar to the discrete time classical random walk discussed in the previous section. However, as mentioned in the previous section, the probabilities regarding the quantum random walk can behave rather strangely. This difference is due to a principle called ”superposition”.

Superposition means that the quantum walk can have, for example, both $\frac{1}{\sqrt{2}}$ 'amplitude' at node 1 **and** $\frac{1}{\sqrt{2}}$ amplitude at node -1. In this case there is, after a measurement, a $|\frac{1}{\sqrt{2}}|^2 = 50\%$ probability to find the walk at node 1 and a 50% probability to find to walk at node -1. But this is not the same as for the classical walk, where the walk was either at node 1 (with 50% chance) **or** at node -1 (with 50% chance). It might seem like almost the same thing, but we will see that this change can lead to big differences, such as destructive interference.

In order to be able to work with the quantum random walk in the next section a few concepts need to be defined. First, the Hamiltonian ”H”. The Hamiltonian of a system defines which nodes are connected with which other nodes. It is a matrix, and (for ring-structures) can be written in an equation as:

$$H = -\gamma \sum_{x=0}^{N} (|x\rangle \langle x+1| + |x+1\rangle \langle x|). \tag{2.1}$$

In equation (2.1) N is number of nodes in the ring, and γ is a constant which is connected to the probability of the quantum random walk to jump from one node to an adjacent node. $|x\rangle$ is a unit-vector corresponding to node ”x” of the system. Usually node 1 corresponds to $|1\rangle = (1, 0, ..., 0)^T$ (where the T stands for transpose), node 2 corresponds to $|2\rangle = (0, 1, 0, ..., 0)^T$ etc. Hence $|x+1\rangle$ is simply $|2\rangle = (0, 1, 0, ..., 0)^T$ if $x = 1$. Finally $\langle x| = |x\rangle^T$.

Taking again the square from figure 2.2 as an example, it follows from definition (2.1) that the corresponding Hamiltonian is

$$H = \begin{pmatrix} 0 & -\gamma & 0 & -\gamma \\ -\gamma & 0 & -\gamma & 0 \\ 0 & -\gamma & 0 & -\gamma \\ -\gamma & 0 & -\gamma & 0 \end{pmatrix}. \tag{2.2}$$

The six constants $-\gamma$ above and below the diagonal indicate the possibility for the walk to jump from node i to node $i+1$ or node $i-1$. The bottom-left and top-right corners indicate jumping from 1 to 4 and jumping from 4 to 1. Importantly we can see from this example that for rings (and in fact for all structures examined in this thesis) the Hamiltonian is real and symmetric.

Using this Hamiltonian we are able to derive the evolution matrix of the probability: G. The derivation is based on the derivation as it is presented in [4].

Suppose the walk starts at a node $|\psi_{in}\rangle$ (for example node 1 on the square) at time $t = 0$. The walk then evolves according to the standard unitary time evolution operator $U(t)$, as follows directly from the Schrödinger equation (we use this because we consider a *quantum* random walk). $U(t)$ is defined as

$$U(t) = e^{-iHt}. \tag{2.3}$$

Just before time $t = \tau$, at time $t = \tau - \epsilon = \tau^-$ with epsilon very small, the walk is then a superposition of nodes given by:

$$\left|\psi(\tau^-)\right\rangle = e^{-iH\tau^-} \left|\psi_{in}\right\rangle. \tag{2.4}$$

This superposition consists of some (or all) of the nodes in the system, and each node $|x\rangle$ in the superposition has an associated probability $P_{|x\rangle,\tau^-}$

$$P_{|x\rangle,\tau^-} = |\left\langle x\middle|\psi(\tau^-)\right\rangle|^2, \tag{2.5}$$

where $\langle x| = |x\rangle^H$, the Hermitian of $|x\rangle$. Since $|x\rangle$ is real in all calculations in this thesis, $\langle x|$ will simply be the transpose.

Now at the same time $t = \tau$ a measurement is performed on the quantum random walk. When a quantum system is measured, it collapses to one of the states in the superposition. In this case the superposition collapses to one of the nodes of the system (for example $|x_1\rangle$):

$$|\psi(\tau)\rangle = |x_1\rangle\,. \tag{2.6}$$

After this measurement the walk is allowed to evolve again until the next measurement at time 2τ:

$$\left|\psi(\tau+\tau^-)\right\rangle = e^{-iH\tau^-}\,|x_1\rangle\,. \tag{2.7}$$

This entire process of evolving and measuring is described by the time-evolution matrix G of the quantum walk:

$$G \equiv \sum_{x,x'\epsilon X} \left|\langle x'|\,e^{-iH\tau}\,|x\rangle\right|^2 |x'\rangle\,\langle x|\,. \tag{2.8}$$

In this sum both x and x' are nodes of the system. X represents the set of all the nodes in this system. τ is a variable called the measurement rate, defined as the time between measurements.

Measurements play an important role in the behaviour of the quantum random walk (In fact, measurements are important in any quantum system). As mentioned, quantum random walks make use of superposition, meaning that they can have amplitudes on several nodes at once. Once this superposition is measured, however, the superposition "collapses", and the quantum random walk is found on one of the nodes which comprised the superposition. Hence if the walk is never measured it will become a superposition consisting of more and more nodes over time. But it is also possible to measure just often enough for the walk to be able to create a small superposition of nearby nodes before collapsing. In this second scenario the quantum walk can be very similar to a classical random walk, while it was very different in the first scenario. We see thus that measurement, and the measurement rate, play an essential role in the behaviour of the quantum random walk.

Having derived the time-evolution matrix G we can now find the probability-vector $|\rho(t)\rangle$ at times $t = \tau n$:

$$|\rho(\tau n)\rangle = G^n\,|\psi_{in}\rangle\,, \tag{2.9}$$

where the notation $|\rho(t)\rangle$ shows that we are considering a column vector. G is the matrix as defined in (2.8), and $|\psi_{in}\rangle$ is the vector representing the starting-node of the walk. If the walk starts at node $|1\rangle$, then $|\psi_{in}\rangle = |1\rangle = \begin{pmatrix} 1 \\ 0 \\ \vdots \\ 0 \end{pmatrix}$. The probability-vector $|\rho(\tau n)\rangle$ is a vector of size N (the amount of nodes in the system), which represents the probability per node of finding the quantum random walk at that node directly after measurement number "n" (hence at time $t = \tau n$). It is important to note that this probability-vector does not indicate a superposition. It indicates the probability of the walk being found at a certain node at a certain time immediately after the collapse of the superposition due to measurement.

3

Return and Transition Problem

In the previous section we derived the evolution of the quantum random walk over time. We use these results in this section to derive the expected amount of measurements $\langle n \rangle$ needed to find the random walk at a particular place, as well as the variance Δn^2. If the node where we want to find the walk is the same as where we started, then this problem is called the 'Return problem' since the random walk returns to where it started. If it is a different node, then we call it the 'Transition problem'.

In order to find $\langle n \rangle$ and Δn^2 for different scenarios a derivation similar to the one from [4] is given below. It is convenient to first derive the probability of detecting the random walk at a certain node $|\psi_{target}\rangle$ *for the first time* at a certain time $t = n\tau$. In a quantum random walk as described in section 2 we had the equation (2.9) for the chance-vector. We modify this equation slightly to account for not finding the walk at the desired node before it is found there for the first time. This causes the new equation for the chance-vector $|\rho(\tau_n)\rangle$ to be:

$$|\rho(\tau_n)\rangle = (G(1 - |\psi_{target}\rangle \langle\psi_{target}|)^{n-1} G |\psi_{in}\rangle . \tag{3.1}$$

This modified equation arises from (2.9) by setting the probability of the walk being found at the desired node to zero after a measurement. This is done since we are only interested in when the walk is found on the desired node *for the first time*. If the walk is found on the desired node then we are done, else the chance of the walk being on the desired node is zero. Therefore, in the next measurement the probability for the walk to have been found on the desired node on any measurement before the current one is always zero.

In order to implement this idea, we use the projection $|\psi_{target}\rangle \langle\psi_{target}|$, and we will define

$$|\psi_{target}\rangle \langle\psi_{target}| \equiv D, \tag{3.2}$$

from now on to save time. Using this new chance-vector, we find the chance of first detection at $|\psi_{target}\rangle$ to be

$$F_n = \langle\psi_{target}|\rho(\tau_n)\rangle = \langle\psi_{target}| (G(1 - D)^{n-1} G |\psi_{in}\rangle . \tag{3.3}$$

Now we can find the expectation value of the number of measurements and its variance using:

$$\langle n \rangle = \sum_{n=1}^{\infty} n F_n. \tag{3.4}$$

This expression is understood as the definition of the expectation value: the sum of all different n multiplied by their corresponding probabilities. In the same way, we express the variance:

$$\Delta n^2 = \langle n^2 \rangle - \langle n \rangle^2. \tag{3.5}$$

We will see that this variance is discontinuous or diverges around the so-called 'exceptional sampling rates' of the quantum random walk.

In order to calculate the value of $\langle n \rangle$ and Δn^2, equations (3.4) and (3.5) could be used directly, but a faster method is available.

By manipulating equation (3.3) appropriately, we will be able to use the z-transform of F_n, increasing the speed of calculation significantly. We start by using induction to show that:

$$(G(1-D))^{n-1}G\left|\psi_{in}\right\rangle = G^n\left|\psi_{in}\right\rangle - \sum_{j=1}^{n-1} F_j G^{n-j}\left|\psi_{target}\right\rangle . \tag{3.6}$$

First, for n=1 both sides of the equal sign are $G\left|\psi_{in}\right\rangle$. Now, assuming that the equality holds for $n-1$, we have:

$$(G(1-D))^{n-2}G\left|\psi_{in}\right\rangle = G^{n-1}\left|\psi_{in}\right\rangle - \sum_{j=1}^{n-2} F_j G^{n-j-1}\left|\psi_{target}\right\rangle$$

$$G(1-D)(G(1-D))^{n-2}G\left|\psi_{in}\right\rangle = G(1-D)G^{n-1}\left|\psi_{in}\right\rangle - G(1-D)\sum_{j=1}^{n-2} F_j G^{n-j-1}\left|\psi_{target}\right\rangle$$

$$= G^n\left|\psi_{in}\right\rangle - \sum_{j=1}^{n-2} F_j G^{n-j}\left|\psi_{target}\right\rangle - (\left\langle\psi_{target}\right| G^{n-1}\left|\psi_{in}\right\rangle - \sum_{j=1}^{n-2} F_j \left\langle\psi_{target}\right| G^{n-j-1}\left|\psi_{target}\right\rangle)G\left|\psi_{target}\right\rangle$$

$$= G^n\left|\psi_{in}\right\rangle - \sum_{j=1}^{n-2} F_j G^{n-j}\left|\psi_{target}\right\rangle - F_{n-1}G\left|\psi_{target}\right\rangle$$

$$(G(1-D))^{n-1}G\left|\psi_{in}\right\rangle = G^n\left|\psi_{in}\right\rangle - \sum_{j=1}^{n-1} F_j G^{n-j}\left|\psi_{target}\right\rangle .$$

Note that the last equality is our equation for n. Hence we have shown equation (3.6) using induction.

This implies the equivalent expression for F_n:

$$F_n = \left\langle\psi_{target}\right| G^n\left|\psi_{in}\right\rangle - \sum_{j=1}^{n-1} F_j \left\langle\psi_{target}\right| G^{n-j}\left|\psi_{target}\right\rangle . \tag{3.7}$$

As indicated before, we work towards the Z-transform of F_n. The Z-transform is defined as:

$$Z\{F\}(z) \equiv \sum_{n=1}^{\infty} F_n z^n. \tag{3.8}$$

Combining equation (3.7) with the new definition (3.8) we obtain:

$$Z\{F\}(z) = \frac{\left\langle\psi_{target}\right| Z\{G\}(z)\left|\psi_{in}\right\rangle}{1 + \left\langle\psi_{target}\right| Z\{G\}(z)\left|\psi_{target}\right\rangle}, \tag{3.9}$$

equivalently:

$$Z\{F\}(z) = \frac{\sum_{n=1}^{\infty} z^n \left\langle\psi_{target}|\rho_{in}(\tau n)\right\rangle}{\sum_{n=0}^{\infty} z^n \left\langle\psi_{target}|\rho_{target}(\tau n)\right\rangle}. \tag{3.10}$$

In both (3.9) and (3.10) the Z-transform of G, $Z\{G\}(z)$ is used. Importantly, this Z-transform can be rewritten using the geometric series:

$$Z\{G\}(z) = \sum_{n=1}^{\infty} G^n z^n = \frac{1}{1-zG} - 1 = \frac{zG}{1-zG}. \tag{3.11}$$

Now that the Z-transform of F_n is introduced, it can be seen from the definition (3.8) and (3.4) that:

$$\langle n \rangle = \sum_{n=1}^{\infty} nF_n = \frac{d}{dz} Z\{F\}(z)|_{z=1}, \tag{3.12}$$

and

$$\langle n^2 \rangle = \sum_{n=1}^{\infty} n^2 F_n = \frac{d}{dz}(z\frac{d}{dz}Z\{F\}(z))|_{z=1}. \tag{3.13}$$

Equations (3.12) and (3.13) are general, but can be made more specific for some scenarios.

3.1. Return Problem

The goal of the return problem is to find the quantum random walk in the same node as it started. Therefore, the return problem is defined such that $|\psi_{in}\rangle = |\psi_{target}\rangle$. This equality simplifies many of the equations, as we will see in the following. In the case that $|\psi_{in}\rangle \neq |\psi_{target}\rangle$, the problem is called the 'Transition problem'. This problem is discussed briefly in the appendix. It is also shown in the appendix that G is (usually) a real Hermitian matrix. It follows that the eigenvectors of G are orthogonal, and thus $|\psi_{in}\rangle$ and $|\psi_{target}\rangle$ are expressible in terms of the eigenvectors of G:

$$|\psi_{in}\rangle = |\psi_{target}\rangle = \sum_{\lambda} \sum_{k=1}^{g_\lambda} \langle \lambda_k | \psi_{in} \rangle \, |\lambda_k\rangle \, . \tag{3.14}$$

Where g_λ is the geometric multiplicity of eigenvalue λ of G, and $|\lambda\rangle$ is the eigenvector corresponding to λ.

Combining this new equality with equations (3.12) and (3.13), we obtain:

$$\langle n \rangle = \frac{1}{\sum_{k=1}^{g_1} |\, \langle \psi_{in} | 1_k \rangle \,|^2}, \tag{3.15}$$

and

$$\Delta n^2 = \langle n \rangle + \langle n \rangle^2 + \langle n \rangle^3 (-2 \sum_{\lambda=1,\Lambda=1} |\, \langle \psi_{in} | \lambda \rangle \,|^2 |\, \langle \psi_{in} | \Lambda \rangle \,|^2 + 2 \sum_{\lambda=1,\Lambda\neq 1} |\, \langle \psi_{in} | \lambda \rangle \,|^2 |\, \langle \psi_{in} | \Lambda \rangle \,|^2 \frac{\Lambda}{1-\Lambda}), \tag{3.16}$$

with both λ and Λ eigenvalues of G, and $|\lambda\rangle$ and $|\Lambda\rangle$ the corresponding eigenvectors. The notation $|1_k\rangle$ is used to denote an eigenstate corresponding to an eigenvalue $\lambda_k = 1$. This is a general result for the return problem, which is correct both in the case of 'exceptional sampling rates' and in the case of any other sampling rate. For 'non-exceptional sampling rates', however, the expression can be further simplified still. The definition of exceptional sampling rates, and the simplification which can then be made, are shown in the next subsection.

3.1.1. Non-exceptional sampling rates

In the case of a non-exceptional sampling rate, equation (3.15) is always the same, as there is then only one eigenvalue which is equal to one. This is the definition which will be used for exceptional sampling rates in this thesis:

$$g_1(\tau) > 1 \Leftrightarrow \tau \text{ is an exceptional sampling rate} \tag{3.17}$$

Thus for non-exceptional sampling rates there is at most one eigenvalue equal to one (since G is real and symmetric). It turns out that there is also always at least one eigenvalue of G equal to one. The eigenstate corresponding to this eigenvalue is

$$|\phi\rangle = \frac{1}{\sqrt{|X|}} \sum_{x \in X} |x\rangle \, . \tag{3.18}$$

The fact that this eigenstate always exists and corresponds to eigenvalue 1 can be understood by considering the form of the state. It is comprised of all nodes in the system with equal amplitude. Therefore this state is what is called the 'mixed state' of the system. The walk is perfectly 'distributed' over all nodes, and hence the probability distribution of the walk will not change when it is allowed to evolve according to time-evolution matrix G:

$$G\left|\phi\right\rangle = \left|\phi\right\rangle = \frac{1}{\sqrt{|X|}} \sum_{x \in X} \left|x\right\rangle . \tag{3.19}$$

See also figure 4.3. Here the probability of the walk being found in node 2 is plotted for a quantum walk which starts in the mixed state on a two node system ($\frac{1}{2}\left|1\right\rangle + \frac{1}{2}\left|2\right\rangle$). The probability for the walk to be found on node 2 stays $\frac{1}{2}$ for any time-step, just like we claimed.

By definition, then, from (3.18) $\left|\phi\right\rangle$ is an eigenstate of G with eigenvalue $\lambda = 1$. With this information, for non-exceptional sampling rates, (3.15) reduces to:

$$\langle n \rangle = \frac{1}{\sum_{k=1}^{g_1} |\left\langle \psi_{in} | 1_k \right\rangle|^2} = \frac{1}{|\left\langle \psi_{in} \middle| \frac{1}{\sqrt{|X|}} \sum_{x \in X} \left|x\right\rangle \right\rangle|^2} = |X|. \tag{3.20}$$

This equation is much simpler than (3.15), $\langle n \rangle$ is simply equal to the number of nodes in the system.

Similarly, for non-exceptional sampling rates, equation (3.16) reduces to:

$$\Delta n^2 = |X|^2 - |X| + 2|X|^2 \sum_{\lambda \neq 1} \sum_{k=1}^{g_\lambda} |\left\langle \psi_{in} | \lambda_k \right\rangle|^2 \frac{\lambda}{1-\lambda}. \tag{3.21}$$

3.1.2. Exceptional sampling rates

For exceptional sampling rates there is by definition at least one more eigenstate with corresponding eigenvalue equal to one. Unfortunately, these eigenstates differ per system (and there are often even several per system), and thus they have to be determined case-by-case. Hence there are no simpler equations for this case than (3.15) and (3.16).

4

Quantum random walks on elementary structures

In this chapter, the derived expressions from the past two chapters are applied to quantum walks on several elementary structures. For some smaller structures (especially rings) the software 'Maple' is used to find analytical solutions to the equations from chapters 2 and 3. For larger structures the expressions become too complicated to solve with Maple, and so they are solved numerically using 'Python'. It is also checked that the analytical and numerical solutions agree for the three node line.

4.1. Analytical approach

As mentioned, an interesting structure to analyse the quantum random walk on is the ring. It will be seen in this chapter that the properties of the walk chance drastically depending on the number of nodes in the ring and the rate at which the walk is sampled. Of course, in any ring the nodes are connected in a ring-like structure, which means the Hamiltonian of the system is:

$$H = -\gamma \sum_{x=0}^{N} (|x\rangle \langle x+1| + |x+1\rangle \langle x|). \tag{4.1}$$

We can diagonalise H to find G, the evolution matrix of the probability. More concretely, G is described by

$$|\rho(\tau n)\rangle = G^n |\psi_{in}\rangle . \tag{4.2}$$

Here, $|\rho(\tau_n)\rangle$ is the probability vector containing the chance of collapsing to a node after measuring. We can determine this G using the following equation.

$$G = \sum_{x,x' \epsilon X} \left|\langle x'| e^{-iH\tau} |x\rangle\right|^2 |x'\rangle \langle x| . \tag{4.3}$$

4.1.1. The Two node "ring"

Let us explore the 'Two node ring', schematically drawn in figure 4.1. For the Two node 'ring' (which is the same system as the Two node 'line'), the Hamiltonian H is defined as:

$$H = \begin{pmatrix} 0 & -\gamma \\ -\gamma & 0 \end{pmatrix}. \tag{4.4}$$

We diagonalise H:

$$H = \begin{pmatrix} 0 & -\gamma \\ -\gamma & 0 \end{pmatrix} = \begin{pmatrix} -1 & 1 \\ 1 & 1 \end{pmatrix} \begin{pmatrix} \gamma & 0 \\ 0 & -\gamma \end{pmatrix} \begin{pmatrix} -1/2 & 1/2 \\ 1/2 & 1/2 \end{pmatrix}. \tag{4.5}$$

We can make use of this diagonalisation to calculate $e^{-iH\tau}$:

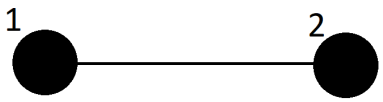

Figure 4.1: Visual representation of the 'Two node ring'. Nodes are drawn as discs, while connections are drawn as lines.

$$e^{-iH\tau} = e^{-i\tau\begin{pmatrix}0 & -\gamma\\ -\gamma & 0\end{pmatrix}} = \begin{pmatrix}-1 & 1\\ 1 & 1\end{pmatrix}\begin{pmatrix}e^{-i\tau\gamma} & 0\\ 0 & e^{i\tau\gamma}\end{pmatrix}\begin{pmatrix}-1/2 & 1/2\\ 1/2 & 1/2\end{pmatrix}. \tag{4.6}$$

With this we can find G:

$$G = \sum_{x,x'\epsilon X} \left|\langle x'|\, e^{-iH\tau}\, |x\rangle\right|^2 |x'\rangle\langle x| \tag{4.7}$$

$$= \sum_{x,x'\epsilon X} \left|\langle x'| \begin{pmatrix}\cos(\tau\gamma) & -i\sin(\tau\gamma)\\ -i\sin(\tau\gamma) & \cos(\tau\gamma)\end{pmatrix} |x\rangle\right|^2 |x'\rangle\langle x| = \begin{pmatrix}\cos^2(\tau\gamma) & \sin^2(\tau\gamma)\\ \sin^2(\tau\gamma) & \cos^2(\tau\gamma)\end{pmatrix}. \tag{4.8}$$

Now we can calculate the chance-vector $|\rho(\tau n)\rangle$ using equation (4.2). If we start the walk at node two, then $|\psi_{in}\rangle = (\begin{smallmatrix}0\\1\end{smallmatrix})$, hence after 1 time-step (at $t = \tau$):

$$|\rho(\tau)\rangle = G\,|\psi_{in}\rangle = (\sin^2(\tau\gamma), \cos^2(\tau\gamma))^T. \tag{4.9}$$

Since the probability for the walk to be found on any node is $\sin^2(x) + \cos^2(x) = 1$, this chance-vector is normalised as expected.

Now, still with initial position $|\psi_{in}\rangle = (\begin{smallmatrix}0\\1\end{smallmatrix})$, we can calculate the chance-vector after n time-steps (so at $t = n\tau$):

$$|\rho(\tau n)\rangle = G^n\,|\psi_{in}\rangle = \left(-\frac{(2\cos^2(\tau\gamma)-1)^n}{2} + \frac{1}{2}, -\frac{((2\cos^2(\tau\gamma)-1)^n + 1)(\cos^2(\tau\gamma)-1)}{2\sin^2(\tau\gamma)} + \frac{1}{2}\right)^T. \tag{4.10}$$

Interestingly, this vector is π-periodic in $\tau\gamma$. This result will be something we see more often, so I introduce the shorthand notation $\tau\gamma = y$. Because of the periodicity, on this structure $\tau\gamma = y$ will give the same result as $\tau\gamma = y + \pi$, as can be seen in equation (4.10) and in figure 4.2. Here, the probability of finding the quantum random walk at the second node (the starting node) is plotted against the amount of time-steps $x = \frac{t}{\tau}$ (not to be confused with the node-vector $|x\rangle$), and the product $\tau\gamma = y$. The plot is shown both as a 3D graph, and as a 2D colour plot, but the information is equivalent. It can be clearly seen that for increasing time the probability to be found at vertex 2 goes to $p = \frac{1}{2}$ for any y as expected, except for some 'special' values of y. For $y \approx \frac{1}{2}\pi$ we see an oscillating behaviour of the probability in x, indicating that for these values of y the quantum random walk 'jumps' between the two vertices.

If the starting position is changed to $|\psi_{in}\rangle = (\frac{1}{2}, \frac{1}{2})$, then we already start off in the limit situation of the previous case. Since the limit is still the same, we stay in this situation for ever. This situation is shown in figure 4.3.

Using equations (3.20) and (3.21) we can determine the expected number of measurements $\langle n\rangle$ before the walk returns to the starting node, as well as the associated variance Δn^2 (for non-exceptional sampling rates). Since there are two nodes is the structure, we immediately find that:

$$\langle n\rangle = 2. \tag{4.11}$$

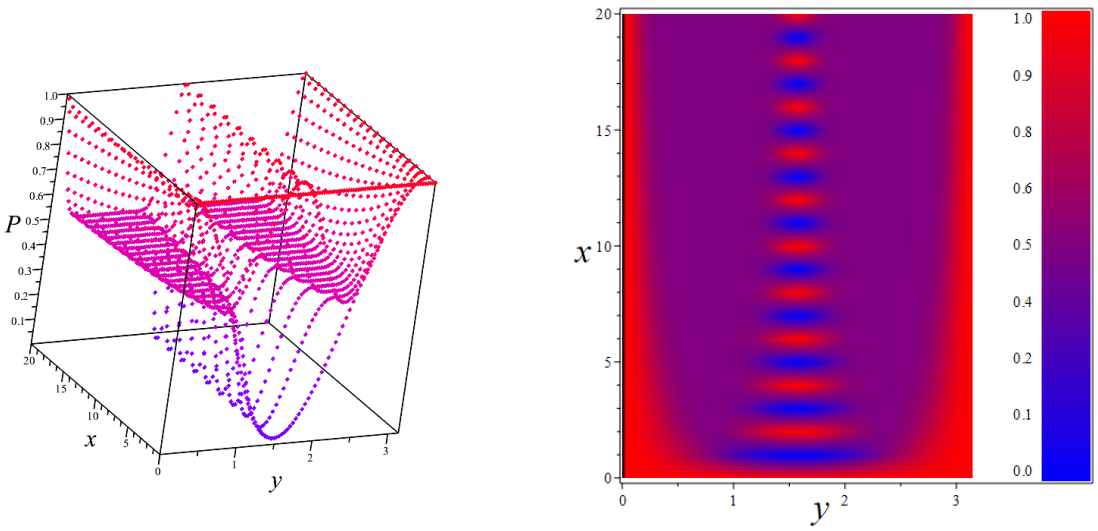

Figure 4.2: The probability of finding the quantum random walk on the second node of the 2 node ring is plotted against the time-step variable x and the product $\tau\gamma = y$. The starting position is $|\psi_{in}\rangle = \binom{0}{1}$. Critical sampling can be seen for $y = k\pi$, and oscillating behaviour for $y = \frac{1}{2}\pi + k\pi$. For other values of y the quantum walk converges to the 'mixed state' where the walk is found on both nodes with probability $\frac{1}{2}$.

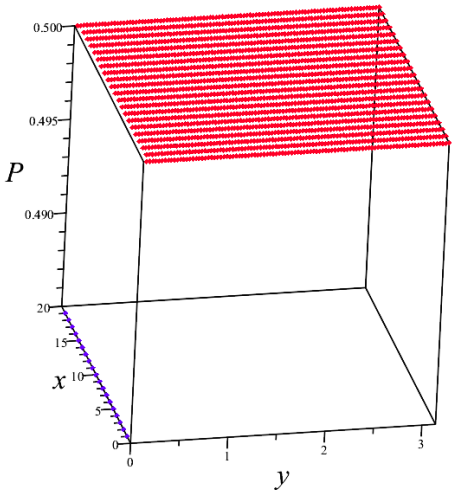

Figure 4.3: The probability of finding the quantum random walk on the second node of the 2 node ring is plotted against the time-step variable x and the product $\tau\gamma = y$. The starting position is $|\psi_{in}\rangle = \begin{pmatrix} 1/2 \\ 1/2 \end{pmatrix}$. As we expect, the probability of finding the walk on either node does not change over time, since we already start out in the 'mixed state' $\begin{pmatrix} 1/2 \\ 1/2 \end{pmatrix}$.

It can be shown that the eigenvalues of (4.7), with corresponding eigenvectors, are:

$$\lambda_1 = 1 \qquad |\lambda_1\rangle = \frac{1}{\sqrt{2}}\binom{1}{1}$$
$$\lambda_2 = \cos(2y) \qquad |\lambda_2\rangle = \frac{1}{\sqrt{2}}\binom{-1}{1},$$

where the factor $\frac{1}{\sqrt{2}}$ is a normalisation factor.

An example of a calculation of the eigenvalues of G on a ring structure can be found in chapter 5.

We thus find that

$$\Delta n^2 = 2 + \frac{4\cos(2y)}{1-\cos(2y)}, \tag{4.12}$$

for non-exceptional sampling rates. At exceptional sampling rates $\cos(2y) = 1$, since the multiplicity of the eigenvalue $\lambda = 1$ has to be greater than or equal to two. Therefore, for rates near the exceptional sampling rates, the variance Δn^2 will diverge towards infinity.

For determining $\langle n \rangle$ at the exceptional sampling rates we can use (3.15) and (3.16). At these rates

$$\langle n \rangle = 1. \tag{4.13}$$

This result corresponds perfectly to the results we found in figure 4.2. At exceptional sampling rates ($y = k\pi$) the walk has probability 1 of being found at node 1 for any x, and hence we expect that the node is found here at the first measurement. We could then expect that the variance for this sampling rate is zero. Is this correct? According to (3.16): Yes. For exceptional sampling rates on the two node 'ring':

$$\Delta n^2 = 0. \tag{4.14}$$

This is a discontinuity, since the variance approaches infinity near this exceptional sampling rate. The critical sampling rate corresponding to the walk staying at the node where it starts is one that is found on every structure and is called the 'Zeno limit'. This is the limit of $\tau \to 0$, or in the figure 4.2 $y \to 0$. Intuitively measurements are then performed so rapidly that the quantum walk does not have time to 'move' to a different superposition than the one it starts out from (in this case node 2).

Another interesting class of sampling rates is $y = \frac{1}{2}\pi + k\pi$. At these rates, the walk 'jumps' back and forth between nodes one and two. This definite behaviour can be recognised in the variance. These rates are namely the only other rates where $\Delta n^2 = 0$.

4.1.2. The Three node ring

The 'Three node ring' is another elementary system, shown schematically in 4.4. The three node ring

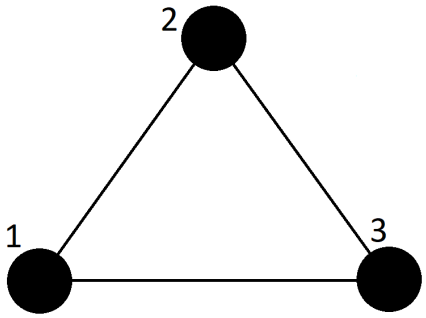

Figure 4.4: Visual representation of the 'Three node ring'. Nodes are drawn as discs, while connections are drawn as lines. Numbers 1, 2, 3 are assigned arbitrarily. It can be seen that due to symmetry the probability distribution on nodes 2 and 3 will be equal when the walk starts out on node 1.

can be solved analogously to the two node system. In figure 4.5 the probabilities are visible for the first and second vertex. A 'ripple' is visible in both figures for x small with $y \approx \frac{1}{3}\pi$, indicating an oscillating behaviour which quickly converges to equal probability on all nodes. The convergence to the mixed state at first glance seems faster than in the two vertices case. Due to symmetry the probabilities at the third vertex are equal to those at the second one, therefore the figure of the probability for the walk to be found on this node is omitted.

Exceptional sampling rates can be seen at $y = \frac{2}{3}k\pi$. This result is confirmed as an example of calculation by hand in chapter 5. The eigenvalues and corresponding eigenvectors of G are also found in this chapter. The result is:

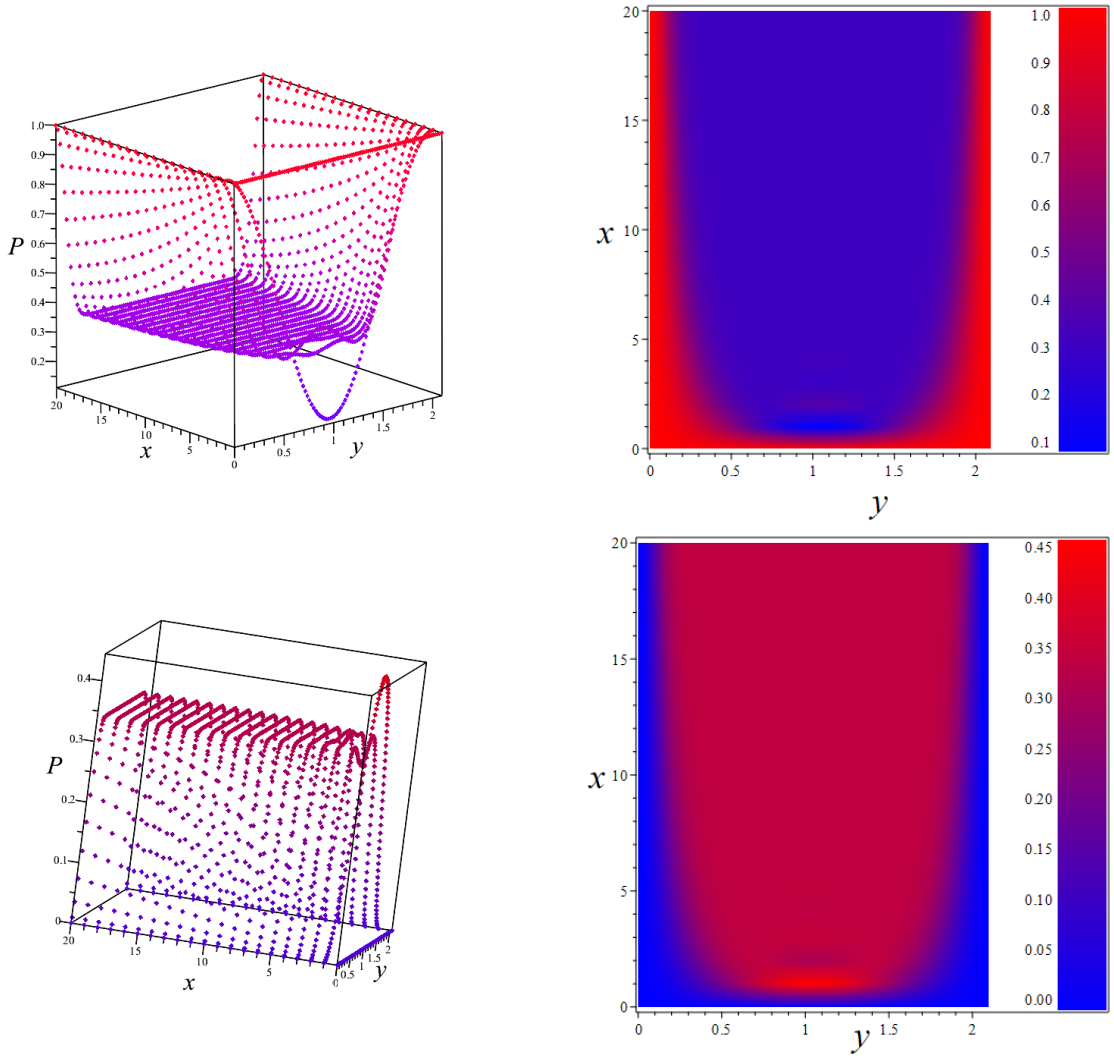

Figure 4.5: The probability of finding the quantum random walk on the first and second node, respectively, of the 3 node ring is plotted against the time-step variable x and the product $\tau\gamma = y$. The starting position is $\psi_{in} = \begin{pmatrix} 1 \\ 0 \\ 0 \end{pmatrix}$. Exceptional sampling is recognised at $y = \frac{2}{3}k\pi$, where the probabilities stay equal to one and zero respectively. For other rates the probability converges to the mixed state of $p = \frac{1}{3}$ on all nodes.

$$\lambda_1 = 1 \qquad |\lambda_1\rangle = \frac{1}{\sqrt{3}}\begin{pmatrix} 1 \\ 1 \\ 1 \end{pmatrix}$$
$$\lambda_2 = \frac{1}{3} + \frac{2}{3}\cos(3y) \qquad |\lambda_2\rangle = \frac{1}{\sqrt{2}}\begin{pmatrix} -1 \\ 1 \\ 0 \end{pmatrix}$$
$$\lambda_3 = \frac{1}{3} + \frac{2}{3}\cos(3y) \qquad |\lambda_3\rangle = \frac{1}{\sqrt{2}}\begin{pmatrix} -1 \\ 0 \\ 1 \end{pmatrix}.$$

Using this, for non-exceptional sampling rates we find that

$$\langle n \rangle = 3, \tag{4.15}$$

and

$$\Delta n^2 = 6 + 4\frac{1 + 2\cos(3y)}{2 - 2\cos(3y)}. \tag{4.16}$$

Once again the variance diverges near exceptional sampling rates, where by definition $\lambda_2 = \lambda_3 = \frac{1}{3} + \frac{2}{3}\cos(3y) = 1$ (and thus $2\cos(3y) = 2$). On average, the variance Δn^2 is larger on this structure

than it was on the two node 'ring'. Intuitively this makes sense, since there are more nodes that the walk can be found on.

As mentioned the exceptional sampling rates are $y = \frac{2}{3}k\pi$. At these sampling rates (3.15) and (3.16) give us:

$$\langle n \rangle = 1, \tag{4.17}$$

as we would expect. Since the quantum random walk will never leave the first node we should find it after one measurement. This is again the Zeno limit. For the same reason we expect (and also find using (3.16)):

$$\Delta n^2 = 0. \tag{4.18}$$

The result for the variance is again zero. It should have been expected that the result for the variance is the same as in the two node 'ring' case, since in both cases the exceptional sampling rate means that the quantum walk never leaves its starting node.

4.1.3. The Four node ring

The 'Four node ring' is a ring structure, similar to the Three node ring, but with an extra node. A schematic drawing can be found in figure 4.6a. The probability of finding the quantum random walk on

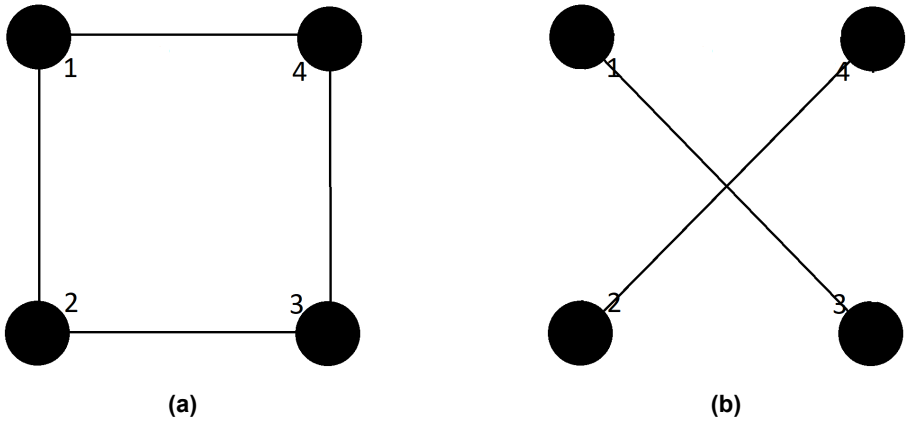

Figure 4.6: A visual representation of the 'Four node ring'. Nodes are drawn as discs, while connections are drawn as lines. Numbers 1, 2, 3, 4 are assigned arbitrarily. It can be seen that due to symmetry the probability distribution on nodes 2 and 4 will be equal when the walk starts out on node 1. In the second figure, the 'breaking' of the Four node ring at critical sampling rate $\tau\gamma = \frac{1}{2}\pi + k\pi$ is shown.

the first, second and third node, respectively, of the 4 node ring is plotted against the time-step variable x and the product $\tau\gamma = y$ in figure 4.7. The starting position is $|\psi_{in}\rangle = \begin{pmatrix} 1 \\ 0 \\ 0 \\ 0 \end{pmatrix}$. Due to symmetry the probability for the walk to be found on node 2 is equal to the probability for the walk to be found on node 4, and thus this the figure corresponding to this node is omitted.

Notice that at $y = k\pi$ and at $y = \frac{1}{2}\pi + k\pi$ critical sampling rates are visible. $y = k\pi$ is the Zeno limit which we have seen before, but at $y = \frac{1}{2}\pi + k\pi$ a new type of critical sampling rate is visible. At this y-value the probabilities of the nodes 1 and 3 behave like they are a two-node system, while the probabilities of vertices 2 and 4 are always zero (they also behave like a two node system, but the quantum random walk starts in the other system). This 'breaking' of the structure into several substructures is a property exclusive to the quantum random walk with no similarities to the classical random walk. It occurs due to destructive interference in the superposition of the walk. Here, for example, the walk gets to node 2 from 1, but also via 3. If the sampling rate τ is just right (in this case if $\tau\gamma = \frac{1}{2}\pi + k\pi$), then the contributions from these two directions will perfectly cancel each other. This means that it becomes impossible for the quantum random walk to ever reach node 2 (and also node 4), as the superposition will never include these nodes.

The breaking of a structure into sub-structures is a property we will see on other structures as well. For the four node ring it is schematically drawn in figure 4.6b.

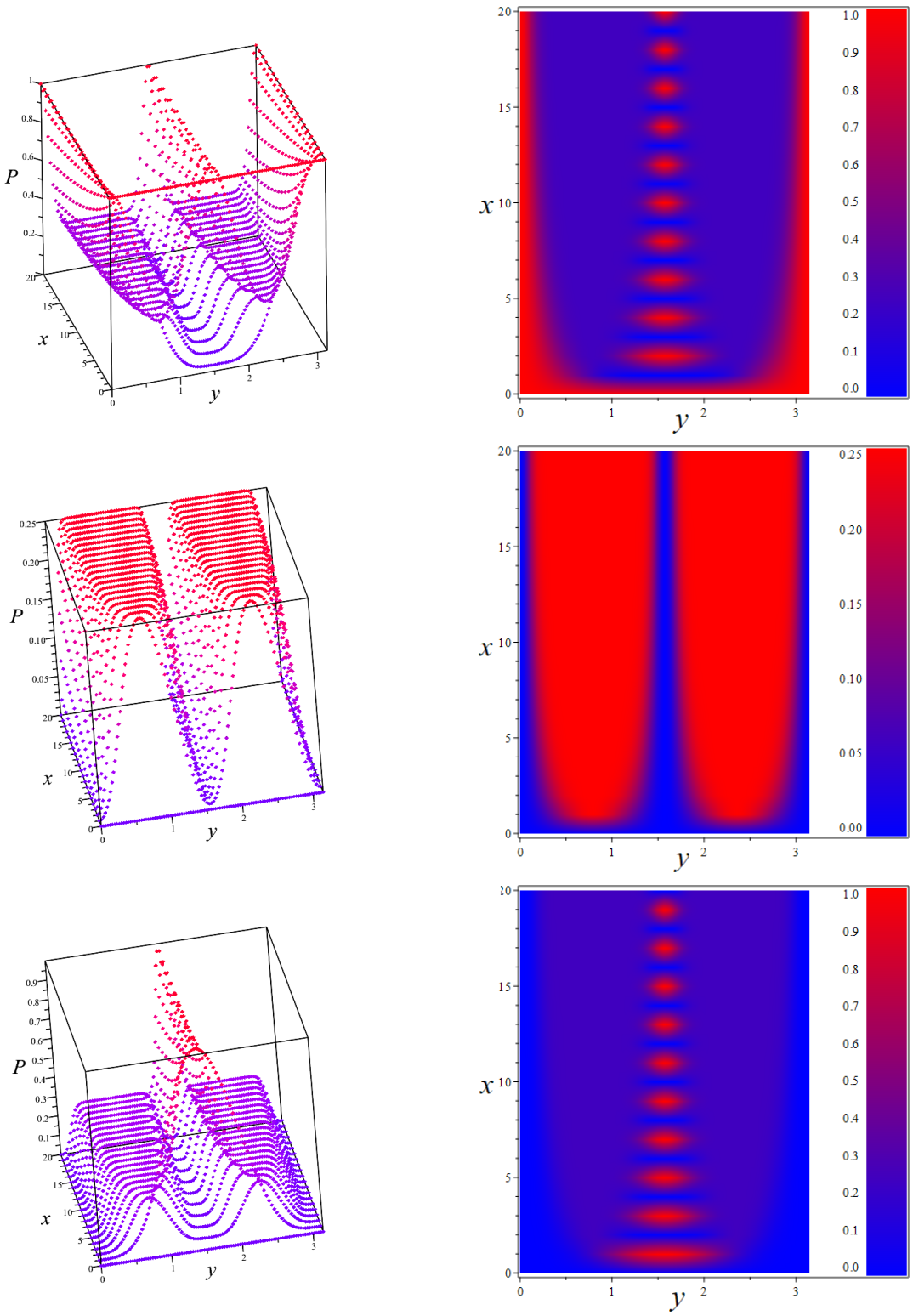

Figure 4.7: The probability of finding the quantum random walk on the first, second and third node, respectively, of the 4 node ring is plotted against the time-step variable x and the product $\tau\gamma = y$. The starting position is $\psi_{in} = \begin{pmatrix} 1 \\ 0 \\ 0 \\ 0 \end{pmatrix}$. Exceptional sampling is recognised at $y = \frac{1}{2}k\pi$. $y = k\pi$ corresponds to the Zeno limit, while $y = \frac{1}{2}\pi + k\pi$ corresponds to the breaking of the four node ring into two pieces.For other rates the probability converges to the mixed state of $p = \frac{1}{4}$ on all nodes.

$\langle n \rangle$ and Δn^2 can be calculated as before. We make use of the fact that the eigenvalues and corresponding eigenvectors of the matrix G of this structure are:

$$\begin{aligned} \lambda_1 &= 1 & |\lambda_1\rangle &= \frac{1}{2}\begin{pmatrix} 1 \\ 1 \\ 1 \\ 1 \end{pmatrix} \\ \lambda_2 &= \cos^2(2y) & |\lambda_2\rangle &= \frac{1}{2}\begin{pmatrix} -1 \\ 1 \\ -1 \\ 1 \end{pmatrix} \\ \lambda_3 &= \cos(2y) & |\lambda_3\rangle &= \frac{1}{\sqrt{2}}\begin{pmatrix} 0 \\ -1 \\ 0 \\ 1 \end{pmatrix} \\ \lambda_4 &= \cos(2y) & |\lambda_4\rangle &= \frac{1}{\sqrt{2}}\begin{pmatrix} -1 \\ 0 \\ 1 \\ 0 \end{pmatrix}. \end{aligned}$$

Since there are four nodes in this system, $\langle n \rangle$ is easily found for non-exceptional sampling rates:

$$\langle n \rangle = 4, \tag{4.19}$$

and for Δn^2 we find:

$$\Delta n^2 = 12 + 8\left(\frac{\cos^2(2y)}{1-\cos^2(2y)} + \frac{\cos(2y)}{1-\cos(2y)}\right). \tag{4.20}$$

This variance is larger (on average) than the variance of the three node ring, continuing the pattern of increasing variance. It is interesting to note that the variance can diverge towards infinity due to the first term in between brackets but also due to the second term in between brackets. These two different options arise due to the two different exceptional sampling rates that the system has.

So there are two different critical sampling rates, and for both of them $\langle n \rangle$ and Δn^2 can be calculated. This calculation has to be done separately since we do not expect the different critical sampling rates to have the same results.

For $y = k\pi$ (the Zeno limit) $\cos(2y) = 1$ and we find:

$$\langle n \rangle = 1, \tag{4.21}$$

which is the result we have seen before, and also

$$\Delta n^2 = 0, \tag{4.22}$$

as we have seen before as well. Of course the result is the same because this critical sampling rate means the same thing as before (never leaving the starting node).

However, there is now a second exceptional sampling rate at $y = \frac{1}{2}\pi + k\pi$, where $\cos(2y) = -1$. At this sampling rate we expect different results. The equations give us:

$$\langle n \rangle = 2, \tag{4.23}$$

and

$$\Delta n^2 = 0. \tag{4.24}$$

This is a remarkable result. The values for $\langle n \rangle$ and Δn^2 are exactly the same as they were in the case of the quantum walk on the two node ring with $y = \frac{1}{2}\pi + k\pi$! This corroborates the conclusion that the structure 'breaks' into two pieces.

4.1.4. The Three node line

The 'Three node line' is similar to the Three node ring, but the connection between nodes 1 and 3 broken in this system. Since we argued that the strange properties of the quantum random walk are due to interference via both sides of the ring, we might expect different results on this structure. We will find, however, that even on a non-circular structure the quantum random walk exhibits its unique properties. A schematic drawing of the Three node line is shown in figure 4.8a.

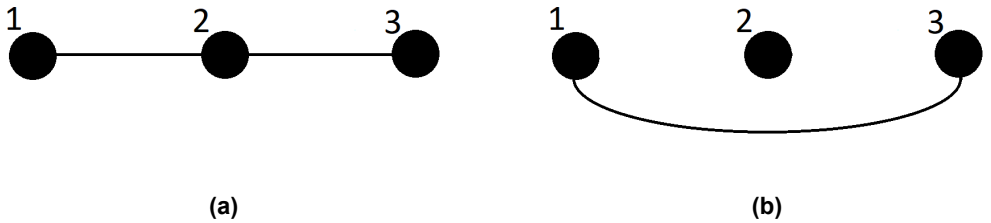

(a) **(b)**

Figure 4.8: A visual representation of the 'Three node line'. Nodes are drawn as discs, while connections are drawn as lines. The second figure shows the breaking of the three node line at critical sampling rate $y = \frac{2}{3}k\pi$.

In figure 4.9 the probability of finding the quantum random walk on the first, second and third node, respectively, of the 3 node line is plotted against the time-step variable x and the product $\tau\gamma = y$. In these figures the starting position of the quantum random walk is $|\psi_{in}\rangle = \begin{pmatrix} 1 \\ 0 \\ 0 \end{pmatrix}$.

Critical sampling rates can be seen at $y = \frac{2}{3}k\pi$. At $y = \frac{4}{3}k\pi$ we recognise the Zeno limit. Hence we expect the same results as before. At $y = \frac{2}{3}\pi + \frac{4}{3}k\pi$ a breaking is recognised. Since the structure is not symmetric in the way the Four node ring was, this is surprising in a way. The break corresponds to node 1 and 3 forming a two node system, while node 2 is excluded and will always have probability zero if the walk starts at a different node. This break is visualised in figure 4.8b. No other break seems possible for this structure. This can be explained using symmetry. We recognise that node 1 and 3 are only different in the name they have been arbitrarily given. If we then search for all symmetrically justified ways of breaking the three node line we find the possibilities:

1. All nodes connected
2. Only node 1 and 3 connected, node 2 excluded
3. All nodes disconnected

These are the possibilities we already found! All nodes disconnected happens in the Zeno limit. The break happens at the other exceptional sampling rates, and all nodes connected is the state of the system at all non-exceptional sampling rates.

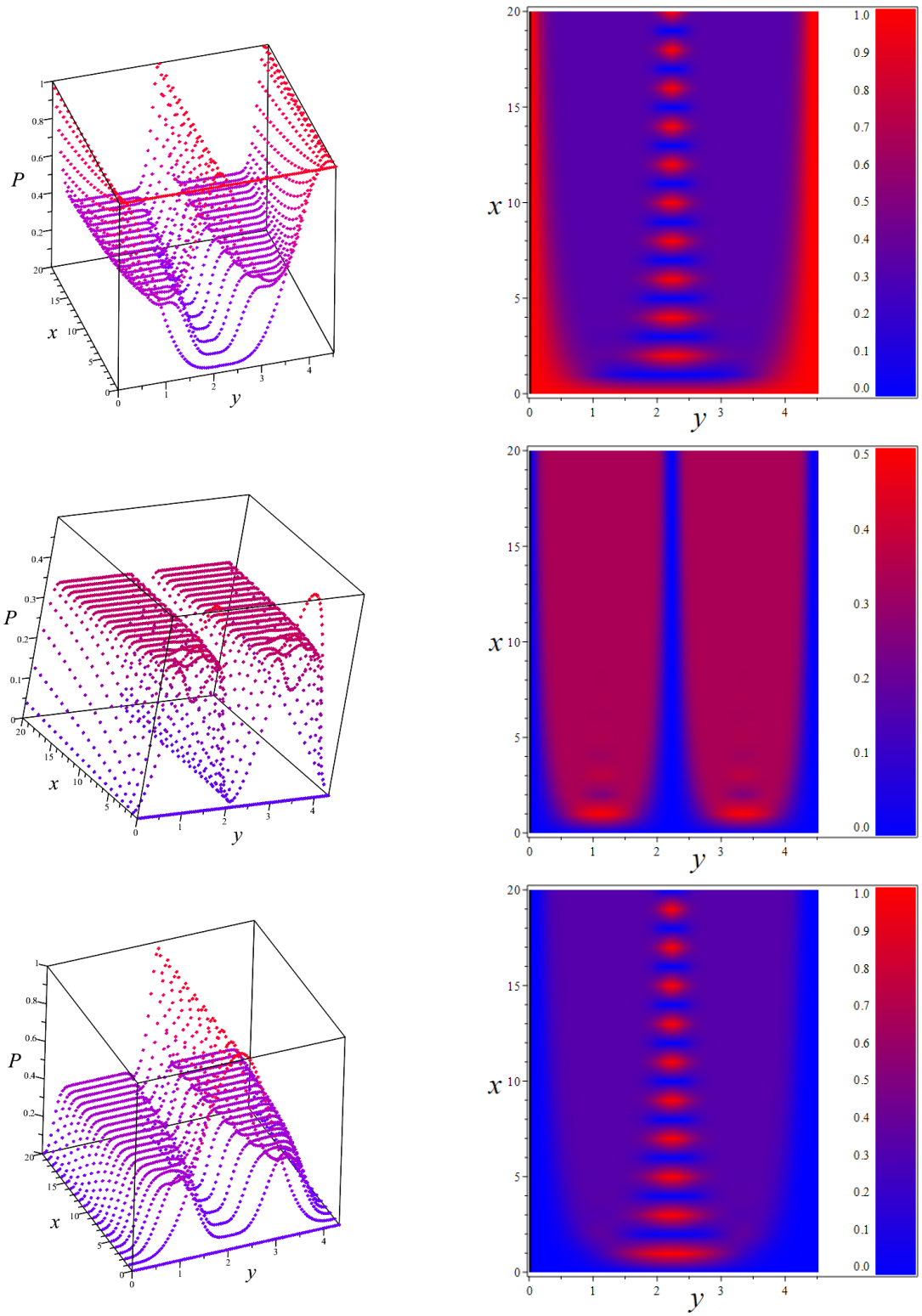

Figure 4.9: The probability of finding the quantum random walk on the first, second and third node, respectively, of the 3 node line is plotted against the time-step variable x and the product $\tau\gamma = y$. The starting position is $\psi_{in} = \begin{pmatrix} 1 \\ 0 \\ 0 \end{pmatrix}$. Exceptional sampling is recognised at $y = \frac{2}{3}k\pi$. $y = \frac{4}{3}k\pi$ corresponds to the Zeno limit, while $y = \frac{2}{3}\pi + \frac{4}{3}k\pi$ corresponds to the breaking of the three node line into two pieces. The structure breaks into a two node system consisting of nodes 1 and 3, and a separated node 2. For other rates the probability converges to the mixed state of $p = \frac{1}{3}$ on all nodes.

4.2. Numerical approach

In the previous section Maple was used to analytically calculate the evolution in time of the probability-vector $|\rho(t)\rangle$ of the quantum walk on simple systems, and we showed the results in a 3D graph as well as in a 2D colour plot. For more complicated systems, however, the computing power required to compute the results in Maple is too large (for my laptop). For these situations we can instead try to find numerical results using Python. The difference in method is that the matrices are multiplied and inverted numerically. Pade approximation is used to calculate the exponential of a matrix[8].

4.2.1. The Two node ring revisited

As a check of the numerical method we first calculate again the results for the two node ring. The probability to find the quantum walk on node 2 is plotted in figure 4.10 for the first two time-steps.

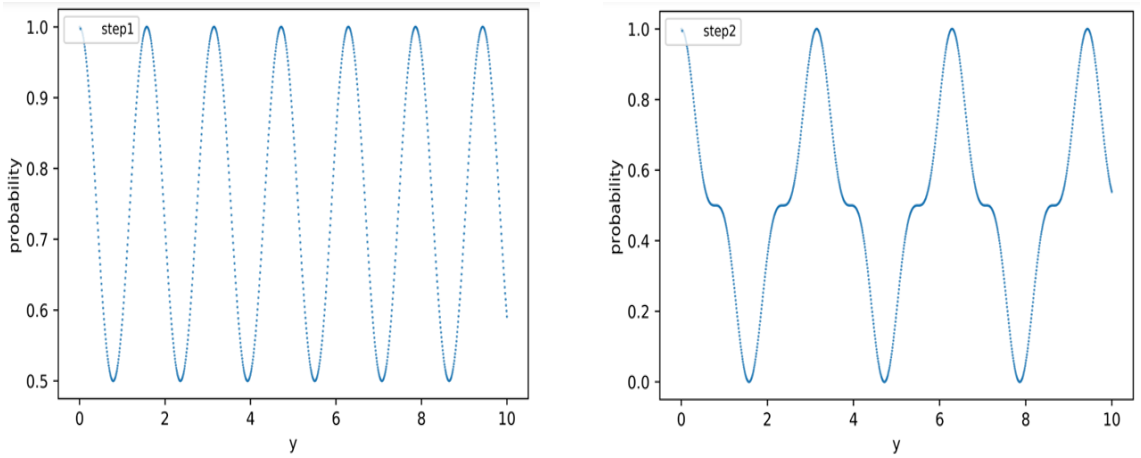

Figure 4.10: The probability of finding the quantum random walk on the second node of the two node ring, on time-steps $x = 1$ and $x = 2$ respectively, is plotted against the product $\tau\gamma = y$. The starting position is $|\psi_{in}\rangle = \binom{0}{1}$. The figures are in a different style than they were in section 4.1 due to the difference in programming language. Comparing these figures to figure 4.2 we see they are the same (as should of course be expected).

It can be seen that the results correspond very well to the analytical solution we found using Maple. The probability is π-periodic in y and is always equal to one at the exceptional sampling $y = k\pi$. At $y = \frac{1}{2}\pi + k\pi$ we see the probability jump from one to zero as we saw before. This gives some confidence in the accuracy of the numerical method.

4.2.2. The Five node ring

Now that we have some confidence in the numerical approximation, we can try to solve larger systems such as the 'Five node ring'. A schematic drawing can be found in figure 4.11. This ring is different from the Four node ring in the sense that five is a prime number. We have seen a prime number ring before (the three node ring, and even the Two node 'ring'), but these rings had very few nodes. We will see that larger prime number rings exhibit different behaviour from what we have seen so far.

Figure 4.12 shows the probability of the quantum random walk to be found on node 1,2,3 respectively after 1 time-step (at $x = 1$, or $t = \tau$). This probability fluctuates wildly as a function of y. There are, however, some higher and lower peaks, and we may suspect that they represent exceptional sampling rates. Another important observation is that on this structure the periodicity of the probability in y is broken. The five node ring is thus the smallest ring which does not exhibit this periodicity in y. Nodes 4 and 5 are not plotted as their probability is equal to nodes 3 and 2 by symmetry.

In figure 4.13 the probability of finding the quantum random walk is once again plotted. The plot is for node 1,2,3 respectively, but at time-step $x = 11$ instead of $x = 1$. It can be seen clearly that the probability converges to $p = 0.2$ for (almost) all y. This result is expected as it represents the mixed state of the quantum random walk on the Five node ring. The only special looking sampling rates which are left are $y = 0$ (which is the Zeno limit, and is always an exceptional sampling rate), $y \approx 5.5$ and $y \approx 8.5$. For $y \approx 5.5$ and $y \approx 8.5$ it is not clear from the figure if these rates represent exceptional sampling rates (meaning that the decay of the peaks is due to the inaccuracies of the numerical method used) or if

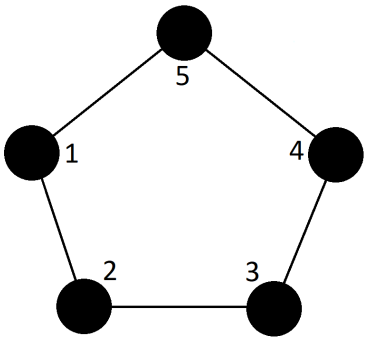

Figure 4.11: Visual representation of the 'Five node ring'. Nodes are drawn as discs, while connections are drawn as lines.

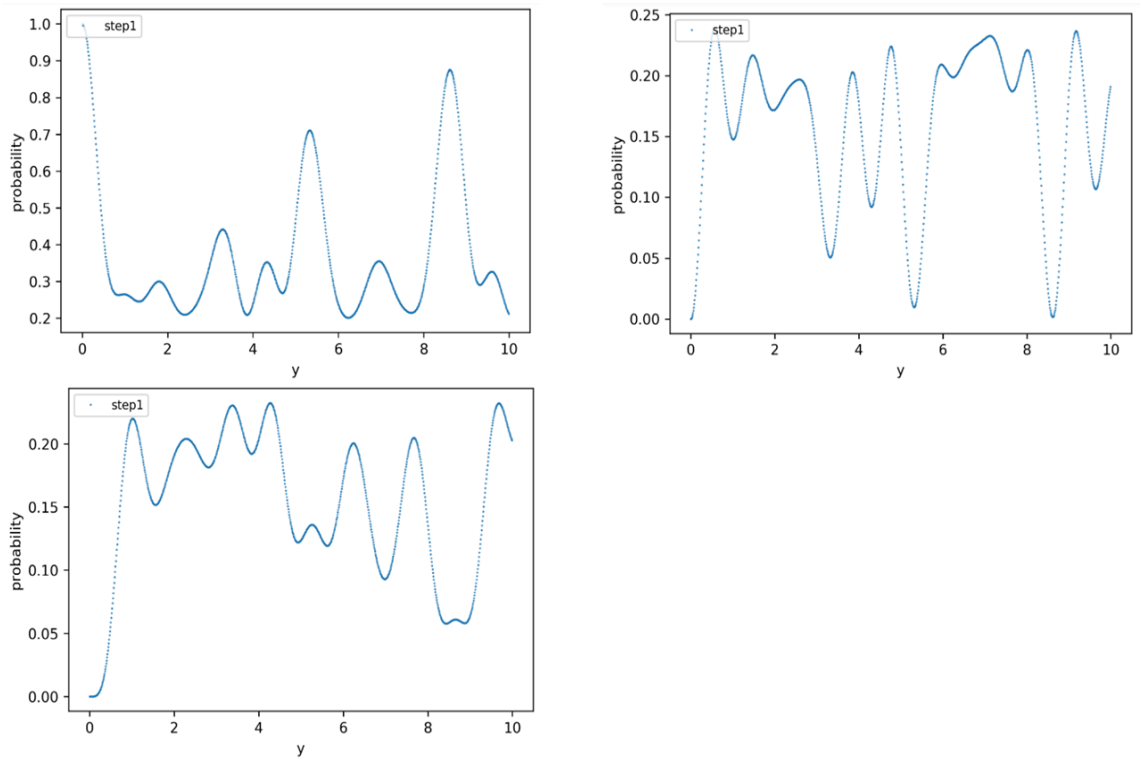

Figure 4.12: The probability of finding the quantum random walk on the first, second and third node, respectively, of the Five node ring on time-step $x = 1$ is plotted against the product $\tau\gamma = y$. Nodes 4 and 5 are not shown since they are equal to nodes 3 and 2 due to symmetry. The starting position is $|\psi_{in}\rangle = \begin{pmatrix} 1 \\ 0 \\ 0 \\ 0 \\ 0 \end{pmatrix}$. The probability is non-periodic in y, causing the probability distribution to look more chaotic than on the smaller structures that we saw before.

the decay of the peaks is the real behaviour of the system (meaning that the peaks are no exceptional samplings rates and hence the Zeno limit is the only exceptional sampling rate of the system).

We will see in the next section (on the six node ring) that the numerical method works very well, which leads us to conclude that the decay of the peaks of the Five node ring is a property of the structure, and not an artefact of the numerical method. This conclusion can also be reached by using the symmetry argument which was introduced in the context of the three node line. Using this argument the only options for breaking of the structure are:

1. All nodes connected
2. All nodes disconnected

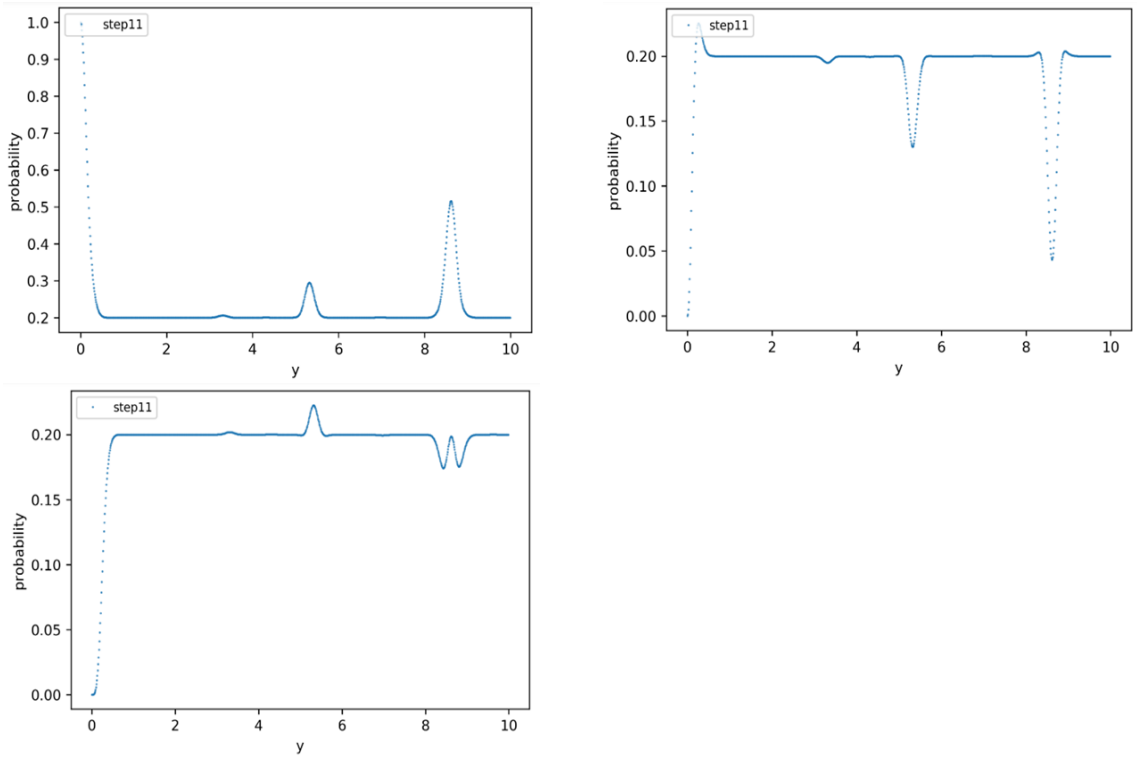

Figure 4.13: The probability of finding the quantum random walk on the first, second and third node, respectively, of the Five node ring on time-step $x = 11$ is plotted against the product $\tau\gamma = y$. Nodes 4 and 5 are not shown since they are equal to nodes 3 and 2 due to symmetry. The starting position is $|\psi_{in}\rangle = \begin{pmatrix} 1 \\ 0 \\ 0 \\ 0 \\ 0 \end{pmatrix}$. The probability is non-periodic in y.

These situations represent the Zeno limit and the non-exceptional sampling rates. Thus we conclude again that the Zeno limit is the only exceptional sampling rate.

4.2.3. The Six node ring

In the analysis of the four node ring we saw that for one exceptional sampling rate the ring 'broke' into two sub-rings, causing the probability at that rate to jump back and forth between 0 and 1. It seems that this breaking into sub-rings is a general property of the ring. In the cases of the two, three, and five node rings the only way to 'break' was into two, three, and five 'rings' consisting of only one node respectively. This happens for every ring at $y = 0$ (the Zeno limit), and for these rings it is the only way to 'break' since their number of nodes is prime.

Non-prime rings such as the six node ring have more ways to break, corresponding to their divisors. A schematic drawing of the six node ring, as well as the possible ways to 'break' has been drawn in figure 4.14. These possible ways to 'break' can be seen very nicely in the evolution with respect to time of the probability for the quantum random walk to be found at node 1. In fig 4.15 this probability is shown at time-step $x = 1$ and at time-step $x = 11$. Peaks can be seen at $y = \frac{2\pi}{1}k, y = \frac{2\pi}{2}k, y = \frac{2\pi}{3}k$. The values correspond to the divisors of six (one, two, three). The height of the peaks converges to $p = 1, p = \frac{1}{2}, p = \frac{1}{3}$, indicating the breaking of the ring into smaller rings of sizes 1, 2, and 3. The last divisor (six) represents the non-exceptional case, and is thus not an exceptional sampling rate. Note also that the probability for the Six node ring is again 2π-periodic in y, which was not the case for the five node ring.

Finally it is visible in this graph that the peaks of the exceptional sampling converge very closely to the height we expect them to have in the long-time case (and they don't decay any further). This suggests that the decay of the peaks in the five node ring was not an artefact of the numerical method, but instead a property of the system.

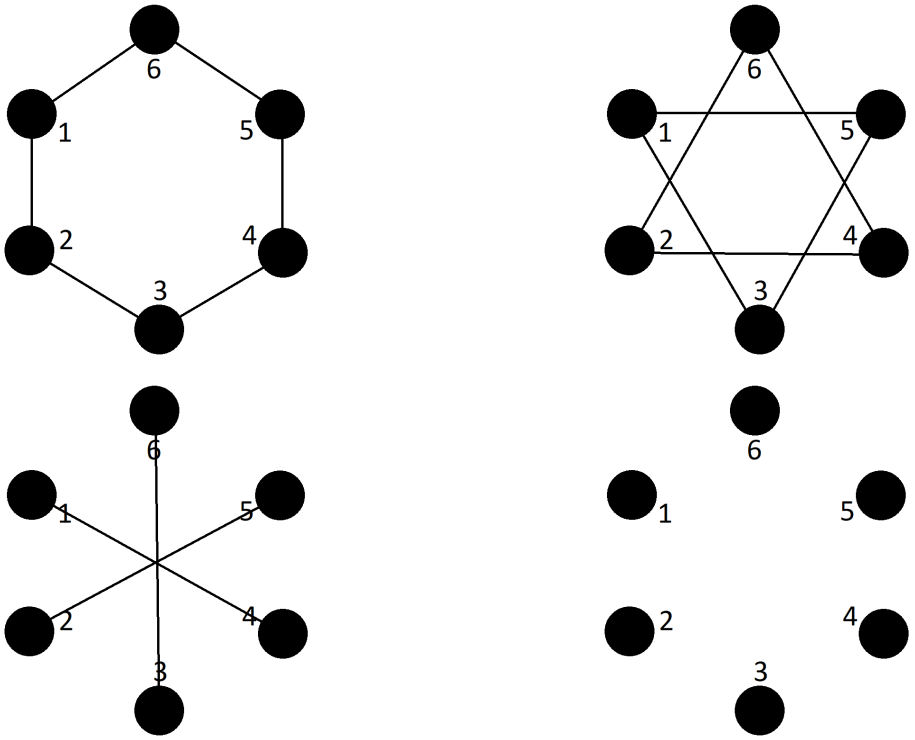

Figure 4.14: Schematic drawing of the possible ways for the Six node ring to 'break' into smaller structures. The amount of nodes in the broken structures corresponds to the divisors of six (six, three, two, one).

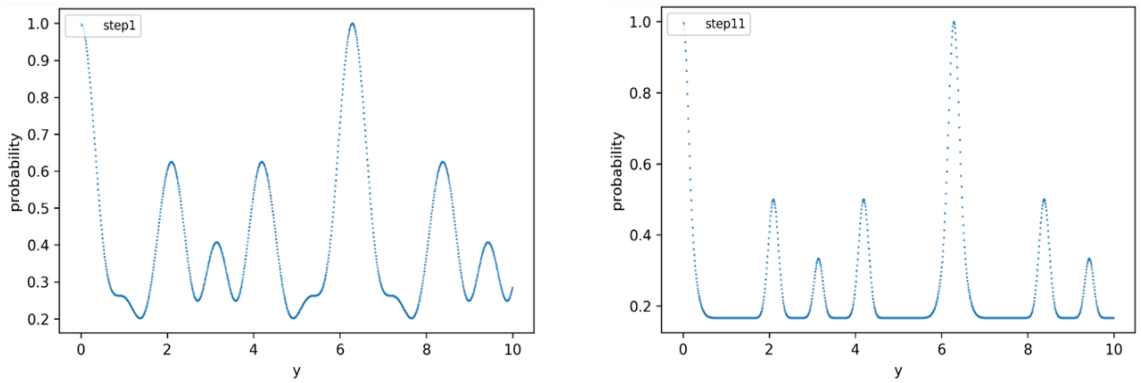

Figure 4.15: The probability to find the quantum random walk at node 1 of the Six node ring is plotted against $\gamma\tau = y$ for time-steps $x = 1$ and $x = 11$. Peaks can be seen at $y = \frac{2\pi}{1}k, y = \frac{2\pi}{2}k, y = \frac{2\pi}{3}k$. The values correspond to the divisors of six (one, two, three). Note that the height of the peaks converges to $p = 1, p = \frac{1}{2}, p = \frac{1}{3}$, indicating the breaking of the ring into smaller structures of one, two, and three nodes. The last divisor (six) represents the non-exceptional case, and is thus not an exceptional sampling rate. The starting position is $|\psi_{in}\rangle = \begin{pmatrix} 1 \\ 0 \\ 0 \\ 0 \\ 0 \\ 0 \end{pmatrix}$.

4.2.4. The Double six node ring

A more complicated structure which can be examined using the numerical method is the 'Double six node ring'. The Double six node ring is a set of two Six node rings, which are connected together by a single connection as shown in 4.16.

The probabilities as calculated by python are shown in figure 4.17 for node one (red in figure 4.16), where the walk is started, and in figure 4.18 for node nine (purple in figure 4.16). In both cases the probabilities are plotted at time-step $x = 1$ and at time-step $x = 10$. It can be seen that the average probability for the walk to be found at node 1 starts out near $p \approx 0.16$ at the first time-step. This is an interesting observation, as this is the probability for the walk to be found at this node in the mixed case

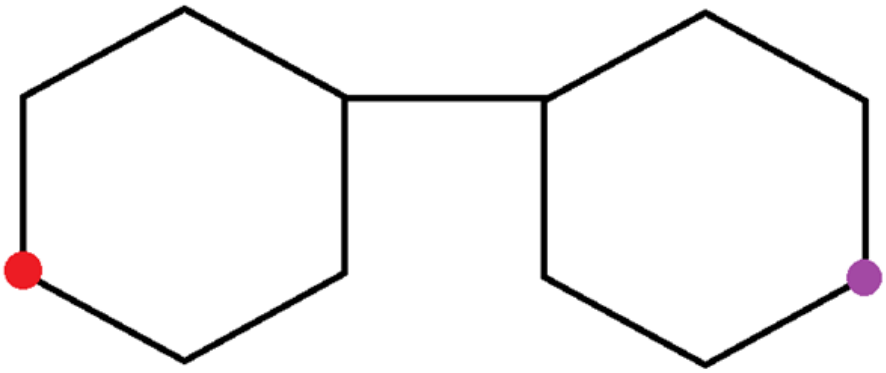

Figure 4.16: The Double six node ring visualised. The red node is called the first node, and the one coloured purple is called the ninth node. These names are arbitrary. It is understood that at every corner of the visualisation a node is present, such that the structure is a combination of two Six node rings.

of a quantum walk on a single Six node ring. At the tenth time-step this average probability drops to slightly below $p = 0.1$. It is expected that for $t \to \infty$ (or equivalently $x \to \infty$) this average probability will converge to $p = 0.083$ when the system approaches the mixed state.

At node nine the probability starts out around $p \approx 0.05$ at the first time-step, but climbs up to above $p = 0.08$ at the tenth time-step. Intuitively, this is due to the quantum random walk slowly mixing from the ring it starts on, through the one connection, with the second ring.

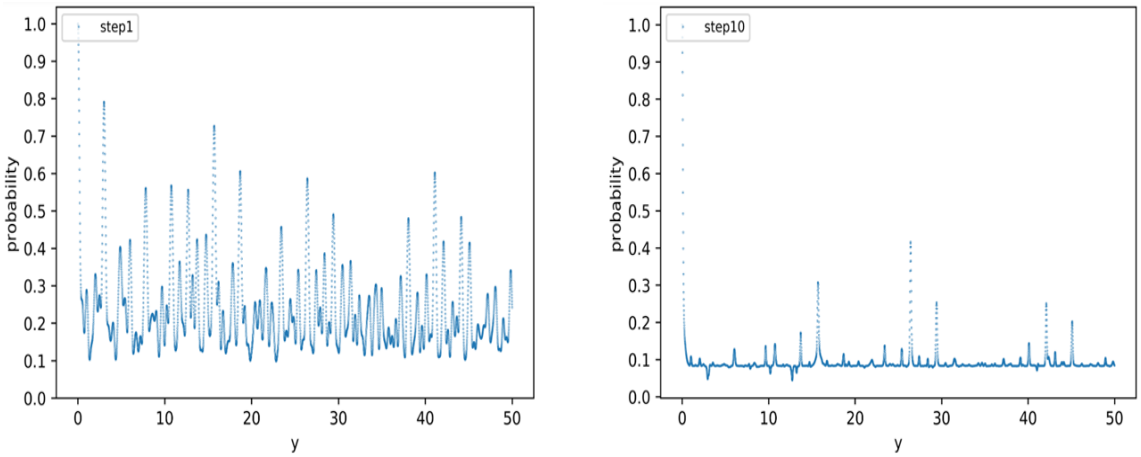

Figure 4.17: The probability of finding the quantum random walk on the first node of the 2 ring system (red), on time-step $x = 1$ and $x = 10$ respectively, is plotted against the product $\tau\gamma = y$. The starting position is $|1\rangle$, and is indicated in red in figure 4.16.

As was the case with the smaller systems, it seems like there might be some exceptional sampling rates. These are indicated by vertical lines in the $x = 10$ plots, and they are especially clear in the figure 4.17. Differently from the small systems, the probability is no longer periodic in y. Due to this loss of periodicity, the plots look a lot more chaotic and random than the graphs we found for the smaller systems (in a way similar to the result for the Five node ring). Since this makes it difficult to recognise the exceptional sampling rates from the probability plots such as 4.17 and 4.18, we raise the question: Can the exceptional sampling frequencies be predicted beforehand, without plotting them numerically? For small rings this was done using Maple, but it can be done by hand as well. This will be the subject of chapter 5, but first the quantum random walk will be analysed on one final structure.

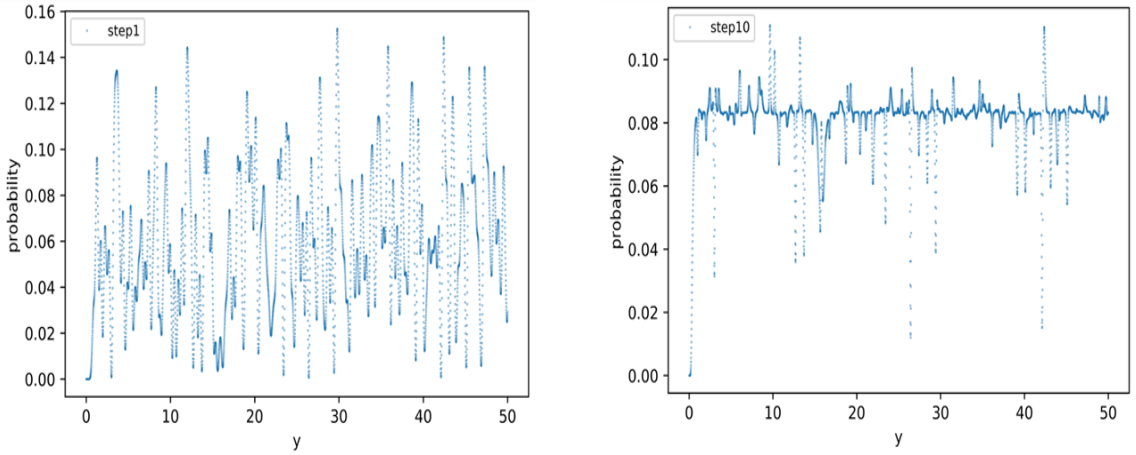

Figure 4.18: The probability of finding the quantum random walk on the ninth vertex of the 2 ring system (purple), on time-step $x = 1$ and $x = 10$ respectively, is plotted against the product $\tau\gamma = y$. The starting position is $|1\rangle$, and is indicated in red in figure 4.16.

4.2.5. The small double tree

The small double tree structure, as shown in figure 4.19 is a structure in which the classical random

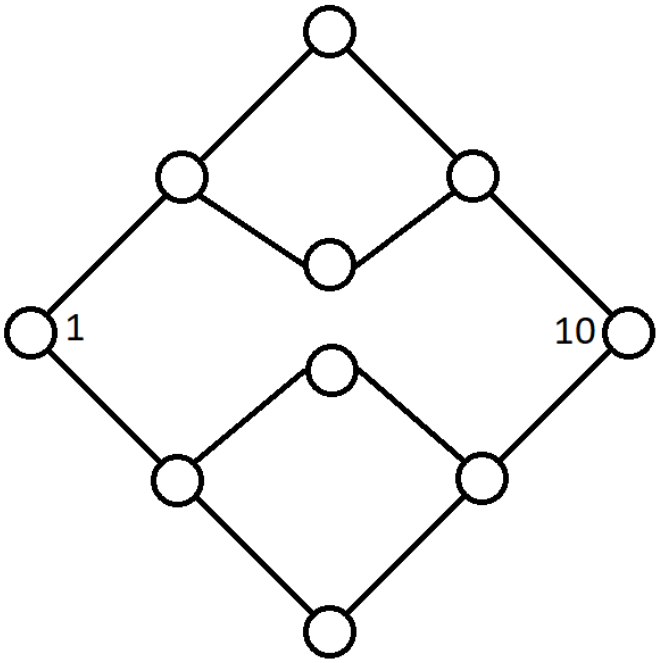

Figure 4.19: The 'small tree' visualised. Nodes are indicated with circles, while connections are shown as lines.

walk is known to get 'stuck'. This is because the probability for the classical random walk is, on every time-step, larger to go to the middle of the structure than to the side. Hence it can take very long for the walk starting on node 1 to reach node 10. See for example [6] and [3].

The quantum random walk can reach node 10 from node 1 much faster. In fact, the numerical calculation of the probability for the walk to be found on nodes 1 and 10 respectively, shown in figure 4.20, illustrates that for $y \approx \frac{2}{3}\pi$ there seems to be an exceptional sampling rate. At this sampling rate the structure 'breaks' as we have seen before. The nodes 1 and 10 form a system similar to the two node system like in section 4.1.1. The situation is not entirely similar, since the probabilities to be found on nodes 1 and 10 jump back and forth between $p = 0$ and $p \approx \frac{1}{2}$ when x increases by 1. Hence there must be a probability of $p \approx \frac{1}{2}$ for the walk to be found on some other node(s) as well.

Therefore, at this sampling rate, the quantum random walk can travel from node 1 to node 10 with 'reasonable' probability in fewer time-steps even than the amount of nodes between node 1 and node 10! One of the reasons that this phenomenon occurs is the fact that the quantum random walk evolves continuously between measurements, and hence the walk is not restricted to jumping only one node per measurement. We thus see that the quantum random walk promises a dramatic improvement of speed over the classical random walk in this case.

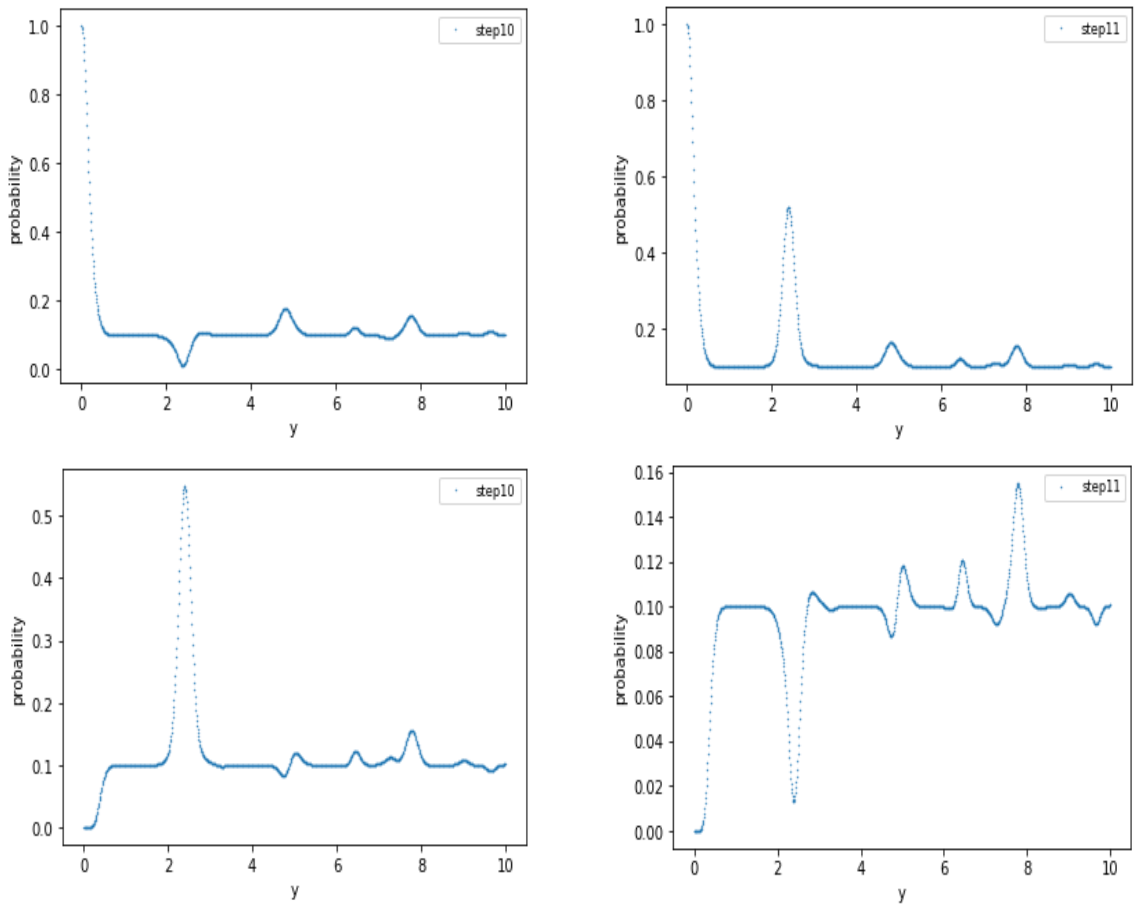

Figure 4.20: The probability of finding the quantum random walk on the first node of the tree-structure, on time-step $x = 10$ and $x = 11$, as well as the probability of finding the quantum random walk on the tenth (final) node of the tree-structure, on time-step $x = 10$ and $x = 11$, is plotted against the product $\tau\gamma = y$. The starting position is the first vertex $|1\rangle$.

5

Finding the exceptional sampling rates

In chapter 4 exceptional sampling rates could often be found easily for the simple systems using Maple (and sometimes Python), but this was not trivial for more complex systems. For this reason we would like to be able to analytically determine the exceptional sampling rates using a different method. By definition an exceptional sampling rate is a rate for which the multiplicity of the eigenvalue 1 of G is greater than one. Hence we need to calculate the eigenvalues of G as a function of the product $\gamma\tau = y$. To make the calculation easier we prove that the matrix G is real and symmetric in the appendix.

5.1. Analytical calculation of the exceptional sampling rates on a ring structure using G

To find the eigenvalues of G we first calculate G. Using equations (4.3) and (4.1) we get an expression for G in the case of an N-sized ring. This equation can take a lot of computing power to solve, but it may be made easier by using the series expansion of the exponential.

As an example I use this expansion in the case of $N = 3$: In this case

$$H = -\gamma \begin{pmatrix} 0 & 1 & 1 \\ 1 & 0 & 1 \\ 1 & 1 & 0 \end{pmatrix}. \tag{5.1}$$

Now we expand $e^{-iH\tau}$ using the Taylor expansion (5.2).

$$e^x = \sum_{n=0}^{\infty} \frac{x^n}{n!}. \tag{5.2}$$

We see:

$$e^{-iH\tau} = \sum_{n=0}^{\infty} \frac{(-iH\tau)^n}{n!} =$$

$$\sum_{n=1}^{\infty} \frac{3^{2n}}{3(2n)!}(-1)^n y^{2n} \begin{pmatrix} 1 & 1 & 1 \\ 1 & 1 & 1 \\ 1 & 1 & 1 \end{pmatrix} + I - \sum_{n=0}^{\infty} \frac{i3^{2n+1}}{3(2n+1)!}(-1)^n y^{2n+1} \begin{pmatrix} 1 & 1 & 1 \\ 1 & 1 & 1 \\ 1 & 1 & 1 \end{pmatrix} =$$

$$\frac{1}{3}\cos(3y) \begin{pmatrix} 1 & 1 & 1 \\ 1 & 1 & 1 \\ 1 & 1 & 1 \end{pmatrix} - \frac{1}{3} \begin{pmatrix} 1 & 1 & 1 \\ 1 & 1 & 1 \\ 1 & 1 & 1 \end{pmatrix} + \begin{pmatrix} 1 & 0 & 0 \\ 0 & 1 & 0 \\ 0 & 0 & 1 \end{pmatrix} - \frac{1}{3}i\sin(3y) \begin{pmatrix} 1 & 1 & 1 \\ 1 & 1 & 1 \\ 1 & 1 & 1 \end{pmatrix} =$$

$$\frac{1}{3} \begin{pmatrix} \cos(3y) - i\sin(3y) + 2 & \cos(3y) - i\sin(3y) - 1 & \cos(3y) - i\sin(3y) - 1 \\ \cos(3y) - i\sin(3y) - 1 & \cos(3y) - i\sin(3y) + 2 & \cos(3y) - i\sin(3y) - 1 \\ \cos(3y) - i\sin(3y) - 1 & \cos(3y) - i\sin(3y) - 1 & \cos(3y) - i\sin(3y) + 2 \end{pmatrix}.$$

Now G is found by squaring this matrix element-wise, resulting in

$$G = \frac{1}{9}\begin{pmatrix} 5+4\cos(3y) & 2-2\cos(3y) & 2-2\cos(3y) \\ 2-2\cos(3y) & 5+4\cos(3y) & 2-2\cos(3y) \\ 2-2\cos(3y) & 2-2\cos(3y) & 5+4\cos(3y) \end{pmatrix}. \tag{5.3}$$

Noting the regular structure of G, we can easily find the eigenvalues in a clever way:

$$\begin{aligned} 0 = \frac{1}{9}\left|\begin{pmatrix} 5+4\cos(3y)-9\lambda & 2-2\cos(3y) & 2-2\cos(3y) \\ 2-2\cos(3y) & 5+4\cos(3y)-9\lambda & 2-2\cos(3y) \\ 2-2\cos(3y) & 2-2\cos(3y) & 5+4\cos(3y)-9\lambda \end{pmatrix}\right| = \\ \frac{1}{9}\left|\begin{pmatrix} 9-9\lambda & 2-2\cos(3y) & 2-2\cos(3y) \\ 9-9\lambda & 5+4\cos(3y)-9\lambda & 2-2\cos(3y) \\ 9-9\lambda & 2-2\cos(3y) & 5+4\cos(3y)-9\lambda \end{pmatrix}\right| = \\ \frac{1}{9}\left|\begin{pmatrix} 9-9\lambda & 2-2\cos(3y) & 2-2\cos(3y) \\ 0 & 3+6\cos(3y)-9\lambda & 0 \\ 0 & 0 & 3+6\cos(3y)-9\lambda \end{pmatrix}\right| = \\ \frac{9-9\lambda}{9}\left|\begin{pmatrix} 3+6\cos(3y)-9\lambda & 0 \\ 0 & 3+6\cos(3y)-9\lambda \end{pmatrix}\right|. \end{aligned}$$

And it follows that

$$\lambda_1 = 1, \tag{5.4}$$

$$\lambda_{2,3} = \frac{1}{3} + \frac{2}{3}\cos(3y). \tag{5.5}$$

From which we deduce that the exceptional sampling rates are the y's such that $\cos(3y) = 1$, hence

$$y = \frac{2}{3}k\pi. \tag{5.6}$$

for any integer k. These results are the same results which were already found using Maple in section 4.1.2, and they can be seen visually in figure 4.5.

Calculation of G's eigenvalues (and thus exceptional sampling rates) for differently sized rings goes in a similar way.

5.2. A simple check of the exceptional sampling rates using H

Another way to look at the exceptional sampling rates is using H. Since G is constructed using H, we expect to be able to predict some of the properties of the walk if we know the structure of H, ideally without explicitly calculating G. In particular, it was postulated in [4] that for any exceptional sampling rate, there is a pair of eigenvalues of H, (λ_1 and λ_2) such that $\lambda_1 - \lambda_2 = 2\pi n$, where $n = 0, 1, 2, 3...$

Unfortunately this property holds only in one direction. Hence we cannot say that if there is a pair of eigenvalues such that their difference is $2\pi n$, then this is an exceptional sampling rate. This means that H can be used as a check to confirm that an exceptional sampling rate is indeed an exceptional sampling rate, but H cannot be used in a self-contained way to determine the exceptional sampling rates directly.

The fact that the property holds only in one direction is illustrated in figure 5.1. Here, the evolution of the eigenvalues λ of the matrix H of the Six node ring system have been plotted as a function of y, where as usual $y = \gamma\tau$. The same eigenvalues have been plotted with added constants of both 2π and 4π. Hence when these lines cross there is a pair of eigenvalues with difference of either 2π or 4π, thus fulfilling the requirement for the sought after property. Unfortunately, as visible in the figure, not all crossings occur at the indicated exceptional sampling rates of $\frac{2}{3}\pi, \pi$ and $\frac{4}{3}\pi$. This confirms that a difference of $2\pi n$ does not always imply an exceptional sampling rate.

It can also be seen that all indicated exceptional sampling rates correspond to at least one crossing. Therefore it is not disproved that the postulated property of H can be used as a check of the correctness of the eigenvalues.

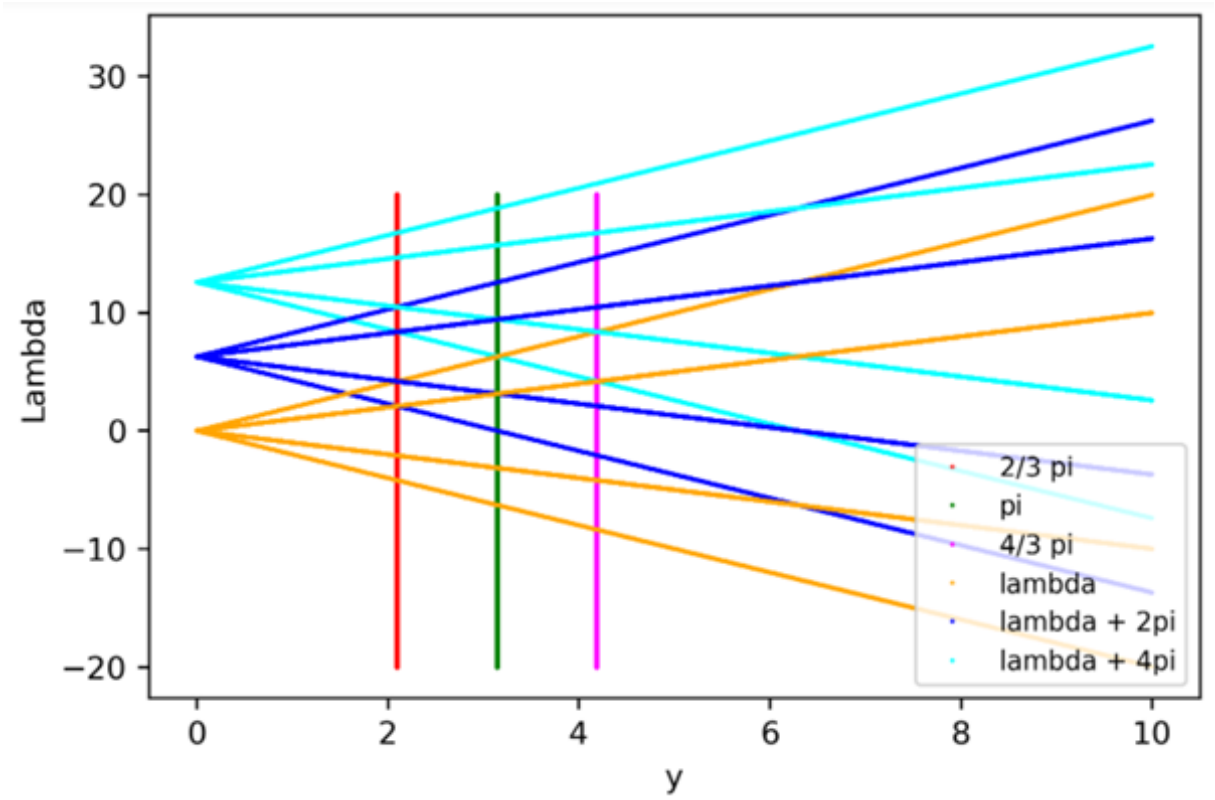

Figure 5.1: In this figure the evolution of the eigenvalues of the matrix H of the Six node ring system have been plotted as a function of $y = \gamma\tau$. The same eigenvalues, but with added constants of respectively 2π and 4π are also plotted. Lastly the first three exceptional sampling rates (excluding $y = 0$) are indicated. Crossings are seen at every sampling rate, but another crossing is found before the exceptional sampling rate $y = \frac{2}{3}\pi$.

6

Conclusion

The behaviour of the discrete time measurement induced quantum random walk has been investigated on many elementary structures, as well as some more complicated ones. In general, it was found that for quantum random walks it is important at what 'sampling rate' measurements are performed. Especially so-called exceptional sampling rates cause behaviour which is drastically different from the classical random walk, as well as from the behaviour of the quantum walk on non-exceptional sampling rates.

On every structure the Zeno-limit was discovered at sampling rate $\gamma\tau = 0$. Intuitively, at this rate of sampling the quantum random walk does not have time to 'move' to any different node than the starting one. For non-prime ring structures it also turned out that there are critical sampling rates corresponding to every divisor of the amount of nodes. At these sampling rates the structure breaks into several smaller structures. Using symmetry, the smaller structures could be predicted accurately in the examples which were examined in this thesis. These critical sampling rates were especially clear for the Six node ring, where they where found using numerical methods, and the same behaviour was found analytically with Maple on the Four node ring. The numerical method was also used for the five node ring, but no clear critical sampling rates (besides the Zeno-limit) where found. This ring is the smallest for which periodicity of the probability in $\gamma\tau$ was broken. Investigating this 'chaotic' behaviour of the five node ring could be the subject of further research.

Similar chaotic behaviour was observed in the probability distribution of the double ring. However, it could be seen that the quantum walk had trouble reaching the second ring. Given enough time, the walk did mix equally over all nodes, as expected. Another interesting structure is the double tree graph. For this structure a possible critical sampling rate was identified which breaks the structure down to a connection between the first and final node (with at least one other node included as well). This break causes the walk to be able to cross from the first node to the final node of the double tree at much faster speeds than the classical random walk. Investigating this breaking for double trees of general size is another interesting possibility for more research.

In general, it has been proved that the evolution matrix G of the quantum random walk is real and symmetric if H is symmetric (which is usually the case). A method has also been outlined to determine the exceptional sampling rates of ring structures analytically, which was confirmed by the findings of the previous chapter of the thesis. Finally, a check has been devised using the eigenvalues of H. Proving this check could be the subject of further research.

References

[1] D. Bouwmeester et al. *Optical Galton board*. 1999. URL: https://journals.aps.org/pra/pdf/10.1103/PhysRevA.61.013410 (visited on 06/02/2022).

[2] Philipp M. Preiss et al. *Strongly correlated quantum walks in optical lattices*. 2015. URL: https://www.science.org/doi/10.1126/science.1260364 (visited on 06/15/2022).

[3] Andrew M. Childs. *Lecture notes on quantum algoritms*. 2021. URL: https://www.cs.umd.edu/~amchilds/qa/qa.pdf (visited on 05/24/2022).

[4] E. Barkai Didi. *Measurement induced quantum walk*. 2021. URL: https://arxiv.org/pdf/2108.13047.pdf (visited on 05/24/2022).

[5] Richard Jozsa and Noah Linden. *On the Role of Entanglement in Quantum-Computational Speed-Up*. 2003. URL: https://www.jstor.org/stable/3560059 (visited on 06/13/2022).

[6] J. Kempe. *Quantum random walks: An introductory overview.* 2008. URL: https://arxiv.org/pdf/quant-ph/0303081.pdf (visited on 05/24/2022).

[7] NOS. *Doorbraak met quantumcomputer van Google 'is echt een mijlpaal'*. 2019. URL: https://nos.nl/artikel/2307353-doorbraak-met-quantumcomputer-van-google-is-echt-een-mijlpaal (visited on 06/13/2022).

[8] SciPy. *Linear Algebra*. 2022. URL: https://docs.scipy.org/doc/scipy/reference/linalg.html (visited on 06/15/2022).

A

Appendix

A.1. Proof that G is real and symmetric

Recall the definition of G:

$$G = \sum_{x,x' \epsilon X} \left| \langle x' | \, e^{-iH\tau} \, |x\rangle \right|^2 |x'\rangle \langle x| \,. \tag{A.1}$$

G is obtained after taking the square of the absolute value of $e^{-iH\tau}$ element-wise. Therefore G is real. Also G is symmetric if $e^{-iH\tau}$ is symmetric. Now we write

$$e^{-iH\tau} = V e^{-iL\tau} V^{-1}, \tag{A.2}$$

where VLV^{-1} is the diagonalisation of H. If we assume that H is symmetric, then even

$$e^{-iH\tau} = V e^{-iL\tau} V^{T}, \tag{A.3}$$

since V is an orthogonal matrix.

It follows that

$$(e^{-iH\tau})^T = V (e^{-iL\tau})^T V^T. \tag{A.4}$$

L is a diagonal matrix of eigenvalues, hence we find

$$(e^{-iH\tau})^T = e^{-iH\tau}, \tag{A.5}$$

and therefore G is symmetric too, as we wanted to show.

A.2. The transition Problem

The goal of the transition problem is to find the quantum random walk on a different node than where it started. Therefore, the transition problem is defined such that $|\psi_{in}\rangle \neq |\psi_{target}\rangle$. In this scenario $\langle n \rangle$ can be derived in the same way as for the return problem. The lack of equality between $|\psi_{in}\rangle$ and $|\psi_{target}\rangle$, however, will result in a far more complicated solution:

$$\langle n \rangle = \frac{\sum_{k=1}^{g_1} \langle \psi_{target} | 1_k \rangle \langle 1_k | \psi_{in} \rangle}{(\sum_{k=1}^{g_1} | \langle \psi_{target} | 1_k \rangle |^2)^2} + \frac{\lim_{z \to 1} g(z)}{(\sum_{k=1}^{g_1} | \langle \psi_{target} | 1_k \rangle |^2)^2}, \tag{A.6}$$

where:

$$g(z) = \sum_{\lambda} \sum_{k=1}^{g_\lambda} \sum_{j=1}^{g_1} \frac{\lambda z}{1 - \lambda z} f(|\lambda_k\rangle, |1_j\rangle), \tag{A.7}$$

and finally:

$$f(|\lambda_k\rangle, |1_j\rangle) = \langle \psi_{target} | 1_j \rangle \langle 1_j | \psi_{in} \rangle \, | \langle \psi_{target} | \lambda_k \rangle |^2 - \langle \psi_{target} | \lambda_k \rangle \langle \lambda_k | \psi_{in} \rangle \, | \langle \psi_{target} | 1_j \rangle |^2. \tag{A.8}$$

This equation can be used directly to determine $\langle n \rangle$ in the case of the transition problem with exceptional sampling rate, but it is very unwieldy. For this reason, the structures in this thesis are analysed using the return problem instead.

A.2.1. Non-exceptional sampling rates

As with the return problem, equation (A.6) can be simplified in the case of non-exceptional sampling. In this case, there is again only one eigenstate with eigenvalue equal to one ($|\phi\rangle$). After some simplification it follows that:

$$\langle n\rangle = |X| + |X| \sum_{\lambda\neq 1}\sum_{k=1}^{g_\lambda} \frac{\lambda}{1-\lambda}(|\langle\psi_{target}|\lambda_k\rangle|^2 - \langle\psi_{target}|\lambda_k\rangle\langle\lambda_k|\psi_{in}\rangle). \tag{A.9}$$

As a check we can fill in $\psi_{target} = \psi_{in}$ into (A.9). The result is that

$$|\langle\psi_{target}|\lambda_k\rangle|^2 - \langle\psi_{target}|\lambda_k\rangle\langle\lambda_k|\psi_{in}\rangle = 0, \tag{A.10}$$

giving again the equality of (3.20) as we would like. The variance can be derived from this expression like it was done in (3.21), but this is quite complicated and not needed for the results in the rest of the thesis.

A.2.2. Exceptional sampling rates

For exceptional sampling rates $\langle n\rangle$ might diverge to ∞, as there is an eigenvalue λ such that $\lambda \to 1$. Then the term $\frac{\lambda z}{1-\lambda z}$ in equation (A.7) diverges to infinity. This is, however, not the only possibility. It is possible as well that the sum $\sum_{j=1}^{g_1}$ is equal to zero, when the terms in $f(|\lambda_k\rangle, |1_j\rangle)$ cancel each other.

Thus, if $f(|\lambda_k\rangle, |1_j\rangle) \neq 0$ for $\lambda_k \to 1$, then $\langle n\rangle$ diverges to infinity. If $f(|\lambda_k\rangle, |1_j\rangle) = 0$ for $\lambda_k \to 1$, then $\langle n\rangle$ can be calculated using a slightly simplified expression from (A.6):

$$\langle n\rangle = (\sum_{k=1}^{g_1}|\langle\psi_{target}|1_k\rangle|^2)^{-1} + (\sum_{k=1}^{g_1}|\langle\psi_{target}|1_k\rangle|^2)^{-2}\sum_{\lambda\neq 1}\sum_{k=1}^{g_\lambda}\sum_{j=1}^{g_1}\frac{1}{1-\lambda}f(|\lambda_k\rangle, |1_j\rangle). \tag{A.11}$$

In this expression the sum over all eigenvalues $\sum_\lambda$ is replaced by a sum over all eigenvalues not equal to one $\sum_{\lambda\neq 1}$. This is justified since we assumed the content of the sum for $\lambda = 1$, $f(|\lambda_k\rangle, |1_j\rangle)$, is equal to zero. An elaborate derivation of this simplification can be found in appendix D of [4].